Nature and Evolution of Primitive Vesuvius Magmas: an Experimental Study

Michel Pichavant, Bruno Scaillet, Anne Pommier, Giada Iacono-Marziano, Raffaello Cioni

Nature and evolution of primitive Vesuvius magmas: an experimental study

MICHEL PICHAVANT[1], BRUNO SCAILLET[1]
ANNE POMMIER[1,2], GIADA IACONO MARZIANO[1]
and
RAFFAELLO CIONI[3]

[1]INSTITUT DES SCIENCES DE LA TERRE d'ORLEANS (ISTO),
UMR 7327, UNIV. ORLEANS, 45071 ORLEANS, FRANCE and
ISTO, UMR 7327, CNRS, 45071 ORLEANS, FRANCE and
ISTO, UMR 7327, BRGM, BP 36009 ORLEANS, FRANCE

[2]SCRIPPS INSTITUTION OF OCEANOGRAPHY, UC SAN DIEGO, 9500 GILMAN DRIVE,
LA JOLLA, CA 92093, USA

[3]DIPARTIMENTO DI SCIENZE DELLA TERRA, UNIVERSITA DEGLI STUDI FIRENZE,
VIA LA PIRA 4, 50121 FIRENZE, ITALY

Submitted to Journal of Petrology

ABSTRACT

Two mafic products from Vesuvius, a tephrite and a trachybasalt, have been crystallized in the laboratory to constrain the nature of primitive Vesuvius magmas and their crustal evolution. Experiments were performed at high temperatures (from 1000 to $\geq$ 1200°C) and both at 0.1 MPa and at high pressures (from 50 to 200 MPa) under H_2O-bearing fluid-absent and H_2O- and CO_2-bearing fluid-present. Experiments started from glass except a few which started from glass plus San Carlos crystals to force olivine saturation. Melt H_2O concentrations reached a maximum of 6.0 wt% and experimental fO_2 ranged from NNO-0.1 to NNO+3.4. Clinopyroxene (Mg# up to 93) is the liquidus phase for the two investigated samples; it is followed by leucite for H_2O in melt < 3 wt%, and by phlogopite (Mg# up to 81) for H_2O in melt > 3 wt%. Olivine (Fo_{85}) crystallized spontaneously in only one experimental charge. Plagioclase was not found. Upon progressive crystallization of clinopyroxene, glass K_2O and Al_2O_3 strongly increase while MgO, CaO and CaO/Al_2O_3 decrease, and residual melts follow the evolution of Vesuvius whole-rocks, from trachybasalt, tephrite, phonotephrite to tephriphonolite. Concentrations of H_2O and CO_2 in near-liquidus 200 MPa glasses and primitive glass inclusions from the literature overlap. The earliest evolutionary stage, corresponding to the crystallization of Fo-rich olivine, was reconstructed by the olivine-added experiments. They show that primitive Vesuvius melts are trachybasalts (K_2O ~ 4.5-5.5 wt%, MgO = 8-9 wt%, Mg# = 75-80, CaO/Al_2O_3 = 0.9-0.95) which crystallize Fo-rich olivine (90-91) as the liquidus phase between 1150 and 1200°C and from 300 to $\leq$ 200 MPa. Primitive Vesuvius melts are volatile-rich (1.5-4.5 wt% H_2O; 600-4500 ppm CO_2 in primitive glass inclusions) and oxidized (from NNO+0.4 to NNO+1.2). Assimilation of carbonate wall-rocks by ascending primitive magmas can account for the disappearance of olivine from crystallization sequences and explains the lack of rocks representative of olivine-crystallizing magmas. A correlation between carbonate assimilation and the type of feeding system is proposed: carbonate assimilation is promoted for primitive magma batches of small volumes; in contrast, for longer-lived, large volume, less frequently recharged, hence more evolved, colder reservoirs, magma-carbonate interaction is limited. Primitive magmas from Vesuvius and other Campanian volcanoes have similar redox states. However, the Cr# of Vesuvius spinels is distinctive and therefore the peridotitic component in the mantle source of Vesuvius differs from the other Campanian magmas.

KEY WORDS: Vesuvius, experimental petrology, phase equilibria, primitive magmas, carbonate assimilation, magma reservoirs, potassic series

INTRODUCTION

Volcanic eruptions of Mt. Vesuvius (Italy) have been conveniently divided into two groups, open-conduit and closed-conduit (e.g., Santacroce et al., 1993; Marianelli et al., 1995). Lava effusion and mixed effusive-explosive activity characterize the former group, which is best illustrated by the 1637-1944 period of activity (Santacroce et al., 1993; Marianelli et al., 1995; 1999; 2005; Scandone et al., 2008). The latter group involves either Plinian or sub-Plinian eruptions with erupted volumes of a maximum of a few km^3, as illustrated by the Pompei (AD 79) and the Pollena (AD 472) eruptions (Cioni et al., 1995; Rosi & Santacroce, 1983). Mafic compositions (tephrite to phonotephrite) typically characterize open-conduit eruptions, and more evolved compositions (tephriphonolite to phonolite) closed-conduit eruptions.

Despite this fundamental subdivision, there is an overall consensus that volcanic activity at Vesuvius is driven by the periodic arrival of primitive mafic magma batches at shallow crustal levels (e.g., Santacroce et al., 1993; Scandone et al., 2008). Mafic magmas are directly emitted together with more evolved, generally crystal-rich products, during violent Strombolian activity, as for example during the 1794, 1822, 1872, 1906 and 1944 eruptions (Marianelli et al., 1995; 1999; 2005; Scandone et al., 2008). In contrast, eruption of mafic magmas is not observed in Plinian events. However, Plinian magma reservoirs such as the AD 79 are periodically recharged by primitive magma batches which contribute energy and mass to the reservoir and mix with the resident differentiates (Cioni et al., 1995). Therefore, it is critical for our understanding of the volcanic activity of Vesuvius to gain a better knowledge of the physical and chemical properties of these primitive magma batches.

So far, information on primitive magma batches at Vesuvius has been quite elusive. Indeed, the absence of primitive products is typical of the activity of Vesuvius (e.g., Dallai et al., 2011). Geochemical studies have stressed the importance of magma mixing in crustal magma reservoirs; most Vesuvius eruption products represent mixtures between mafic and more evolved magmas (e.g., Belkin et al., 1993; Santacroce et al. 1993; Villemant et al., 1993; Marianelli et al., 1999). Up to now, only detailed mineralogical studies have provided clues on Vesuvius primitive magmas. Studies of primitive phenocrysts (Fo-rich olivine and diopside) and of their melt inclusions have documented the occurrence of trachybasaltic to tephritic glasses (MgO = 8-10 wt%; CaO/Al_2O_3 = 1.0-1.1), proposed to be representative of primitive Vesuvius melts (Cioni, 2000; Cioni et al., 1998; Marianelli et al., 1995; 1999; 2005). Volatile concentrations in these glass inclusions (H_2O = 1.5-4.5 wt%, CO_2 = 600-4500

ppm, Cioni, 2000; Marianelli et al., 1995; 1999; 2005) have been used to determine depths of magma crystallization (Marianelli et al., 1999; 2005).

Another approach to constrain the nature of Vesuvius primitive magma is experimental. Experimental petrology is increasingly being applied to active basaltic volcanoes. For Vesuvius, previous high pressure experimental work has concentrated on evolved phonotephritic to phonolitic rocks (Dolfi & Trigila, 1978; Scaillet et al., 2008). One relatively primitive tephrite sample has been experimentally investigated at 0.1 MPa (Trigila & De Benedetti, 1993). In this paper, we report the results of an experimental study on Vesuvius mafic products, as an extension of our earlier work on Vesuvius phonolites (Scaillet et al., 2008). The data constrain the nature and physical conditions (major element composition, crystallization pressures and temperatures, melt volatile concentrations, redox state) of primitive Vesuvius magmas. New arguments for an interaction between primitive magmas and carbonate wall-rocks are provided. A correlation between the extent of carbonate assimilation and the type of feeding system is proposed. Primitive magmas from Vesuvius and the other Campanian volcanic centers (Phlegrean Fields, Ischia, Procida) can be compared. On a broader perspective, this study contributes to the experimental characterization of mafic K-rich magmas which includes rocks such as lamproites, lamprophyres and minettes (Barton & Hamilton, 1978; Esperança & Holloway, 1987; Wallace & Carmichael, 1989; Righter & Carmichael, 1996).

EXPERIMENTAL APPROACH AND SELECTION OF STARTING SAMPLES

In this study, natural mafic products from Vesuvius were equilibrated under controlled laboratory conditions. Most experiments were carried out at high pressures (between 50 and 200 MPa), both under hydrous but H_2O-undersaturated conditions (hereafter designated as fluid-absent, i.e., the melt H_2O content is expected to be less than the solubility) and in presence of a H_2O- and CO_2-bearing fluid phase (hereafter designated as fluid-present, i.e., addition of CO_2 imposes the presence of a fluid phase). In addition, volatile-free experiments were performed at 0.1 MPa. Experimental products were systematically compared with phenocryst assemblages and phenocryst and glass inclusion compositions from eruptive products. In this study, eruptions younger than Avellino (3.9 ka BP) have been considered, in particular Pompei (AD 79), Pollena (AD 472), 1631, the 1637-1944 period and 1906 and 1944.

One major concern at the beginning of this study was the choice of starting materials since, as emphasized above, primitive products are basically lacking at Vesuvius. Another issue is that few mafic Vesuvius products actually represent magmatic liquids because of

magma mixing and phenocryst accumulation or removal (e.g., Marianelli et al., 1999). With these difficulties in mind, two samples were selected, a tephrite (VES9) from a subplinian medieval (8th century) eruption and a trachybasalt (VS96-54A) from the 1944 eruption (Table 1; Fig. 1a). VES9 originates from a lava fountaining episode and is made of fallout crystal-rich (40% crystals) lapilli. Phenocrysts of clinopyroxene (cpx, $Fs_{5-18}En_{34-49}Wo_{46-50}$, calculated with total Fe as Fe^{2+}), leucite (K/(K+Na) = 0.903-0.943) and rare plagioclase (plag, $Ab_{20-53}An_{40-80}Or_{1-7}$) are present, together with a few magnetite (TiO_2 = 11.7 wt%) and apatite inclusions (Table 2). VS96-54A comes from the main layer of the 1944 lava fountain deposits (Marianelli et al., 1999). The sample is porphyritic (45% crystals). It hosts two distinct phenocryst assemblages, the first comprising diopside ($Fs_5En_{48}Wo_{47}$) and Fo-rich olivine (ol, Fo up to 90) and the second salite ($Fs_{9-15}En_{36-43}Wo_{48-50}$), less Fo-rich olivine (Fo_{50-73}), plagioclase ($Ab_{11-16}An_{80-87}Or_{2-5}$) and minor leucite (K/(K+Na) = 0.907-0.914, Table 2; Marianelli et al., 1999).

VES9 (K_2O = 5.55 wt%, Table 1; Fig. 1a) is compositionally close to the "parental mafic magma batch B" of Santacroce et al. (1993), being slightly more primitive than the V36 tephrite investigated by Trigila & De Benedetti (1993). MgO (6.73 wt%) and CaO/Al_2O_3 (0.88) are in the middle of the range of primitive glass inclusions from the 1637-1944 period (Marianelli et al., 1995; 1999; 2005). Compared to VES9, VS96-54A has a higher MgO (7.97 wt%) and CaO/Al_2O_3 (1.04, Table 1), approaching the most primitive 1637-1944 inclusions (Marianelli et al., 1995; 1999; 2005). However, it is less potassic (K_2O = 4.29 wt%) and more calcic (CaO = 13.96 wt%) than VES9 and the primitive inclusion group, suggesting some clinopyroxene accumulation (Marianelli et al., 1999).

Other starting products were considered during the course of the study, but none with clearly superior characteristics was found. In particular, a tephrite / phonotephrite (VS97-718) from a peripheral eruption of pre-medieval age (Table 1; Fig. 1a) was examined in detail. This porphyritic sample contains phenocrysts of diopside ($Fs_{4-5}En_{48-49}Wo_{47-48}$), salite ($Fs_{10-17}En_{32-44}Wo_{46-51}$), Fo-rich (Fo up to 90) olivine with Cr-rich (Cr# up to 81) spinel inclusions, and leucite (K/(K+Na) = 0.916-0.930, Table 2). Geochemically, VS97-718 is close to VES9 (Fig. 1a), being only slightly more magnesian (Table 1). Mineralogically, it is similar to VS96-54A (coexistence of two distinct phenocryst assemblages). Moreover, olivine in VS97-718 is too Fo-rich to be at equilibrium with bulk rock. Therefore, it was not subjected to specific experimental investigations. However, olivines, diopsides and Cr-spinels in VS97-718 are among the most primitive in Vesuvius products and their compositions are given in Table 2.

EXPERIMENTAL METHODS

Starting materials

VES9 and VS96-54A were ground in an agate mortar to ~ 50 μm and fused in air at 1400 °C, 0.1 MPa in a Pt crucible. For each sample, two cycles of melting of 2-4 hours each (with grinding in between) were performed, yielding an homogeneous glass whose composition was checked by electron microprobe (Table 1). The glass was then crushed to ~ 50 μm and stored in an oven.

Most experiments used these two glasses directly as starting materials. A few experiments were conducted with glass (either VS96-54A or VES9) plus San Carlos olivine crystals ($Fo_{90.5}$, sieved to 50-100 μm) to force saturation of the melt with a Fo-rich olivine under the specific experimental conditions.

High pressure experiments

Noble metal capsules, either $Au_{90}Pd_{10}$ or $Au_{70}Pd_{30}$ (more rarely $Ag_{70}Pd_{30}$) > 1050°C and Au ≤ 1050°C, were used as containers (length 15 mm, internal diameter 2.5 mm, wall thickness 0.2 mm). For hydrous but H_2O-undersaturated experiments, amounts of distilled water between 0.6-2 μl and about 30 mg of glass powder (i.e., less water than expected solubilities) were loaded in the capsule. For hydrous but fluid-saturated experiments performed with H_2O-CO_2 mixtures, $Ag_2C_2O_4$ was introduced in the capsule as the source of CO_2, together with distilled water and the glass powder (about 30 mg). H_2O and $Ag_2C_2O_4$ were weighed so as to generate charges with variable $XH_2O_{in.}$ (initial molar H_2O / (H_2O + CO_2)) while the (H_2O + CO_2) / (H_2O + CO_2 + glass) mass ratio was kept constant at ~ 10%. All capsules were sealed by arc welding, keeping them in a liquid nitrogen bath to prevent water loss. They were then put in an oven for several hours and reweighted to check for leaks.

High pressure experiments were all carried out in the same internally heated pressure vessel, working vertically and pressurized with Ar-H_2 mixtures obtained by sequential loading of H_2 and Ar at room temperature (Scaillet et al., 1992). Initial H_2 pressures ranged from 0 (no H_2 initially loaded) to 5 bar. This yielded experimental fH_2 (measured by Ni-Pd-O sensors, see below), from 0.1 to 12 bar (Table 3; 4). Total pressure was recorded by a transducer calibrated against a Heise Bourdon tube gauge (uncertainty ± 20 bar). A double winding Mo furnace was used, allowing near isothermal condition in the 2-3 cm long hot spot (gradient < 2-3 °C/cm). Temperature was measured by three thermocouples (either type S or K) and recorded continuously (total uncertainty ± 5 °C). Run durations were longer for the fluid-

absent (14.5 to 23 h) than for the fluid-present (2 to 7.5 h) experiments. All runs were drop-quenched, resulting in nearly isobaric quench rates of ~ 100 °C/s (Di Carlo et al., 2006).

A majority of runs included a Ni-Pd-O sensor capsule which served to determine the experimental fH_2 (Taylor et al., 1992; Di Carlo et al., 2006; Pichavant et al., 2009). Analysis of the composition of the NiPd alloy after the experiment allows the fO_2 of the sensor capsule to be determined (Pownceby & O'Neill, 1994). The fH_2 of the sensor (and by inference of the experiment since fH_2 is identical for all capsules) is then obtained from the water dissociation equilibrium using the fO_2 determined above, the dissociation constant of water (Robie et al., 1979) and the fugacity of pure water at the experimental P and T (Holloway, 1987). NiPd alloy compositions and the corresponding fH_2 are listed in Tables 3 and 4. For runs performed without a sensor, experimental fH_2 were estimated from the H_2 pressure initially loaded into the vessel, the procedure being calibrated from experiments which included a sensor. For a given experiment (i.e., constant P-T-fH_2), the fO_2 of each individual charge varies along with aH_2O (or fH_2O). The latter was determined for each charge from the H_2O content of the quenched glass, using the thermodynamic model for H_2O solution in multicomponent melts of Burnham (1979). The oxygen fugacity of each charge is then calculated from the water dissociation equilibrium, using the fH_2 and fH_2O determined above, and the dissociation constant of water (Robie et al., 1979). Typical uncertainties on log fO_2 are less than 0.25 log units (e.g. Scaillet et al., 1995; Martel et al., 1999; Scaillet & Evans, 1999; Costa et al., 2004). In this study, fO_2 are expressed as deviations from the NNO buffer (ΔNNO values), calculated at the P and T of interest (Table 3; 4).

At the end of the experiment, capsules were weighed to check for leaks and then opened. For each capsule, fragments of the run product were mounted in epoxy and polished for SEM observations and electron microprobe analyses. Glass chips from selected charges were prepared for FTIR measurements. The metallic pellets in the sensor capsule were recovered, mounted in epoxy and then analyzed by electron microprobe.

0.1 MPa experiments

These were carried out in two vertical gas-mixing furnaces using the wire-loop method. Redox conditions were controlled with CO-CO_2 gas mixtures and the fO_2 (from NNO to NNO+0.5) was directly read using a ZrO_2 electrochemical cell. Temperature was monitored from Pt-PtRh thermocouples. Considerable experimental difficulties were encountered, especially with K_2O volatilization. To minimize K_2O volatilization and, at the same time, Fe loss from the charge to the suspension wire, experiments were repeated under constant T-fO_2 conditions during 2-3

cycles of relatively short durations (3 h, each starting with fresh glass) to progressively saturate the same suspension wire with Fe. Intermediate charges were quenched, then dissolved in HF, and the charge from the last cycle was retained for detailed study (Pichavant et al., 2009). Both Re and Pt suspension wires were tested but Re was found to enhance K_2O volatilization and its use was subsequently avoided.

ANALYTICAL METHODS

All charges were systematically examined by SEM under back-scattered electron mode (JEOL WINSET JSM 6400 instrument, University of Orléans) to assist in the identification of the phases and to evaluate the importance of quench crystallization. Electron microprobe analyses of natural and experimental phases were performed either with the Cameca Camebax, the Cameca SX-50 or the Cameca SX Five of the join BRGM-CNRS-UO facility at Orléans. Analyses were carried out under an acceleration voltage of 15 kV, counting times of 10 and 5 s on peak and background respectively, and a sample current of 6 nA, except for metallic sensor phases which were analyzed under 20 kV and 20 nA. For glasses, a slightly defocused beam of about 5 μm was used, and for minerals a focused beam of 1-2 μm. Silicate minerals were used as standards. For the different oxides, the relative analytical errors are 1 % (SiO_2, Al_2O_3, CaO), 3 % (FeO, MgO, TiO_2) and 5% (MnO, Na_2O, K_2O, P_2O_5). Phase proportions, FeO and K_2O losses were calculated for each charge using a least-squares mass balance routine computed after Albarède (1995), using electron microprobe compositions of the glass starting material and of phases coexisting in the charge. The regression was based on 8 major oxides, excluding MnO, P_2O_5 and H_2O.

One near-liquidus (#5-4) experimental glass was analyzed for dissolved H_2O by Karl-Fischer titration, using equipment and procedures identical to those described by Behrens et al. (1996). This glass was also analyzed for H_2O by FTIR, together with glasses #3-1, #5-1 and #5-2 (fluid-absent experiments), whereas glasses #18-1, #17-2 and #5-3 (fluid-present experiments) were analyzed for both H_2O and CO_2. To do so, a Thermo Fisher FTIR instrument comprising a Nicolet 6700 spectrometer attached to a Continuum microscope was used. Spectra were acquired between 650 and 7000 cm^{-1} on doubly polished glass wafers mostly < 50 μm thick using an IR light source, a KBr beamsplitter and a liquid nitrogen cooled MCT/A detector. Between 2 to 6 spots (aperture mostly 50 μm) were analyzed on each sample. Concentrations of H_2O and CO_2 were determined from the Beer-Lambert law. Densities of experimental glasses were calculated from densities of starting glasses measured

at room conditions (VS96-54A: 2.769 ± 0.008; VES9: 2.703 ± 0.007) and taking a partial molar volume of H_2O of 12 cm^3/mol (Richet et al., 2000). H_2O concentrations were obtained from the absorbance of the 3510-3530 cm^{-1} band, with a linear baseline drawn between 3800 and 2500 cm^{-1}. An extinction coefficient (ε_{3530}) of 67 L/mol.cm was used (Marianelli et al., 1999). For CO_2, the absorbance of the 1515 cm^{-1} band was measured on background-subtracted spectra (Dixon et al., 1995). An extinction coefficient (ε_{1515}) of 365 L/mol.cm (Marianelli et al., 1999) was used.

Most charges had too many crystals to allow analysis of their glass volatile concentrations by FTIR. Therefore, we had to resort to the "by difference" method to estimate the concentration of dissolved volatiles (e.g., Devine et al., 1995). In each electron microprobe session, the difference from 100% of glass electron microprobe analyses was calibrated against the dissolved H_2O content, using glasses of known H_2O concentrations (those analyzed by Karl-Fischer titration and FTIR) as secondary standards. For the fluid-absent (CO_2-free) charges, the calibration is straightforward and glass H_2O concentrations with this method are estimated to within ± 0.5 wt%. For the fluid-present (CO_2-bearing) charges, glass H_2O concentrations are overestimated since CO_2 dissolved in glass increases the difference to 100%. However, in this study, CO_2 concentrations in glasses are < 0.2 wt%. Therefore, the overestimation remains small and the "by-difference" method was also applied to estimate glass H_2O concentrations in CO_2-bearing charges.

EXPERIMENTAL RESULTS

The experiments are divided into three groups, corresponding respectively to the fluid-absent, fluid-present and 0.1 MPa charges. Experimental conditions and results for each group are detailed in Tables 3-5, and experimental compositions are given in Table 6. In total, 19 high pressure (corresponding to 44 charges) and 10 0.1 MPa experiments are reported. All experimental charges were equilibrated under moderately to fairly oxidizing redox conditions. ΔNNO range from -0.1 to +3.4 in the high pressure experiments, and the fluid-absent (ΔNNO = -0.1 to +2.5) and fluid-present (ΔNNO = +0.7 to +3.4) charges overlap. The 0.1 MPa charges are more tightly grouped (ΔNNO = 0 to +0.4).

Fe loss, quench crystallization and evaluation of equilibrium

The importance of Fe loss (due to Fe alloying with the metallic capsule) can be evaluated from the mass balance calculations (Tables 3-5). In the high pressure experiments, 5 charges have > 10% relative Fe loss, including 3 charges with > 20% loss; none has more than 27%

relative Fe loss. At temperatures $\leq$ 1100°C, Fe losses or gains are < 10% relative, except in charge #1-6 (Table 3). At temperatures > 1100°C, Fe loss reaches 21 and 25% relative in charges #3-2 and #3-4 (Table 3). Note, however, that the olivine-added charges were not mass-balanced (because the added olivine crystals were not precisely weighed) and so their Fe losses are unknown. In the 0.1 MPa experiments, 3 charges have Fe losses > 10% and none has more than 19% relative loss. Therefore, Fe loss was kept at relatively low levels in our experiments. No systematic change in phase assemblages or compositions appears between charges with different Fe losses. K volatilization was limited to $\leq$ 10% relative in the 0.1 MPa experiments (Table 5).

Quench phases were commonly detected from SEM observations and their presence is rather systematic in the high-pressure fluid-absent charges (Table 3). In comparison, in the fluid-present charges which are on average less H_2O-rich, quench crystals are rare (Table 4). Quench crystallization is marked by the appearance of very thin needles (most certainly phlogopite) generally forming overgrowths on pre-existing crystals. Quench phases tend to concentrate in crystal-rich regions, and are typically absent from large glass pools. They are also less frequent in crystal-poor charges. Despite their common occurrence, quench phases are rarely abundant enough for their crystallization to have a measurable effect on the melt composition. K_2O loss (which measures quench phlogopite crystallization in high pressure experiments, Di Carlo et al., 2006) is < 10% relative except in two charges (#4-2: 12%; #4-3: 18%, Table 3). It is therefore concluded that quench crystallization is of negligible importance in this study.

Most charges (48) were of crystallization type, whether fluid-absent, fluid-present or volatile-free. In the 6 olivine-added charges (3 fluid-absent and 3 fluid-present), olivine dissolution occurred, either alone or simultaneously with clinopyroxene crystallization. Although no reversals have been performed, several lines of evidence indicate a close approach toward equilibrium in our experiments. (1) Experimental durations were 2-23 h (13.5 h on average, 5-10 h for the olivine-added charges), sufficient for equilibrium crystallization of hydrous basaltic melts (Sisson & Grove, 1993; Barclay & Carmichael, 2004; Di Carlo et al., 2006; Pichavant & Macdonald, 2007). The 0.1 MPa experimental cycles lasted each for relatively short durations (3 h, see above), yet phase assemblages and proportions of crystals are mutually consistent and evolve predictably with temperature (Table 5). (2) Crystal morphologies are euhedral, equant or tabular. The distribution of crystals in both the crystallization and dissolution-crystallization charges is homogeneous; no crystal settling was recognized. The difficulties encountered to quench the charges (see above) can be taken as an

indication for fast crystal nucleation and growth in our experiments. (3) Sums of residuals from mass balance calculations (crystallization charges only) range from values < 0.1 to > 4 (Tables 3-5). 19 charges have $\Sigma R^2 < 0.5$, indicating excellent balance of silicate components between coexisting phases. The highest ΣR^2 values (> 2) correspond to charges with Fe balance problems, either because of Fe loss (the 5 charges with Fe loss > 10% relative) or of Fe gain (because of analytical overestimation, 4 charges have Fe gains > 5 and < 10% relative). (4) Glasses are chemically homogeneous. In the dissolution-crystallization charges, no compositional gradient was detected around the dissolving olivine crystals. (5) Compositions of clinopyroxenes are generally homogeneous. However, in charges #3-4, #2-1, #2-3, #1b-1, #1b-3, standard deviations for clinopyroxene analyses exceed analytical errors for SiO_2, Al_2O_3, FeO and MgO (Table 6). SEM observations reveal core-rim zonation. The dispersion of clinopyroxene-liquid Fe-Mg exchange coefficients reflects these small chemical heterogeneities although, globally, the dataset suggests crystal-liquid equilibrium (see below). (6) Olivine crystallized spontaneously in charge #7-1 is chemically homogeneous with a Fe-Mg exchange coefficient (K_d) suggestive of a close approach toward crystal-liquid equilibrium (see below). In comparison, residual crystals in olivine-added charges did not completely equilibrate under the imposed experimental conditions. At 1150°C, residual olivines have Fo and CaO contents in the same range as the starting San Carlos crystals. For Fe and Mg, olivine-melt equilibration is suggested on the basis of Fe-Mg K_d values (see below) but, for CaO, the residual olivines keep low concentrations inherited from the starting crystals. At 1200°C, both the Fe-Mg K_d values and the CaO contents suggest equilibrium between residual olivine rims and melt (see below).

Phase equilibria

Clinopyroxene, phlogopite, leucite and olivine spontaneously crystallized in the experiments; apatite was occasionally found, but neither plagioclase nor Cr-spinel were encountered. The most important crystalline phase is by far clinopyroxene, present in 48 charges on a total of 54. The clinopyroxene proportion reaches a maximum of 45 wt% in charge # 1-6 (Table 3).

At 0.1 MPa and for a fO_2 between NNO and NNO+0.5, phase assemblages and crystallization sequences are identical for the two compositions investigated. Clinopyroxene is the liquidus phase (Table 5). Liquidus temperatures are between 1222-1212°C for VS96-54A and 1209-1201°C for VES9, significantly lower than previously reported for Vesuvius rocks at 0.1 MPa (from ~ 1260 and up to ~ 1330°C, Trigila & De Benedetti, 1993, their figure 16). In both samples, leucite appears at ~ 1180°C, second to clinopyroxene in the

crystallization sequence. Despite experiments being performed at temperatures below 1180°C and as low as ~ 1125°C (Table 5), the appearance of the third crystalline phase of the 0.1 MPa sequence was not observed.

At high pressures, the phase relations were not completely explored for each pressure because, in the range investigated (50-200 MPa), the influence of pressure is minor, as detailed below. The 200 MPa T-H_2O in melt section for VS96-54A (Fig. 2) illustrates the phase equilibria, which are closely similar for VES9 (not shown). For VS96-54A, clinopyroxene is the liquidus phase. At 1150°C, the liquidus is bracketed by charges #3-1 and #3-2 (Table 3), and the same liquidus phase assemblage (clinopyroxene + liquid) persists at 100 and 50 MPa (charges #15-1 to -4 and #16-1 to -3 respectively, Table 4). At 1100°C, the stable phase assemblage is also clinopyroxene + liquid (Fig. 2). Runs #1 and #2, both performed at 1100°C, 200 MPa (Table 3), show that raising fO_2 by 1-2 log units increases the proportion of clinopyroxene in the charge but leaves the stable phase assemblage unchanged. Contours of clinopyroxene proportions (Fig. 2) exclude the oxidized run #2. The stable phase assemblage is also clinopyroxene + liquid at 100 MPa (charge #6-1, Table 3) whereas in the 50 MPa, 1100°C charge (#7-1, Table 3), olivine occurs together with clinopyroxene. At 1050°C for H_2O-rich conditions, phlogopite joins clinopyroxene in the crystallization sequence (Fig. 2). Phlogopite-bearing charges have melt H_2O concentrations between 5.1 and 6.0 wt% (run #4, Table 3). For near H_2O-saturation, the liquidus temperature for VS96-54A (Fig. 2) is ~ 1120°C, about 100°C lower than at 0.1 MPa.

For VES9, clinopyroxene is also the liquidus phase at 200 MPa. The 1150°C liquidus is half-bracketed by the clinopyroxene + liquid charge #13-2 (Table 4), and the same phase assemblage persists at 100 and 50 MPa (charges #15-5 and #16-4 respectively, Table 4). At 1100°C, clinopyroxene also crystallizes on the 200 MPa liquidus (run #1b, Table 3). The 100 MPa charges demonstrates a shift from clinopyroxene + liquid to clinopyroxene + leucite + liquid when decreasing the melt H_2O content below ~ 3 wt% H_2O (#6-2, #12-5, #12-3, #12-2, Tables 3-4). Clinopyroxene + liquid is the stable phase assemblage at 50 MPa (charge #7-2, Table 3). At 1050 and 1000°C for H_2O-rich conditions, phlogopite joins clinopyroxene both at 200 and 100 MPa (charges #8-1, #9-1 and #10-1, #11-1 respectively, Table 3).

In summary, the high pressure near-liquidus phase equilibria are deceptively simple. Clinopyroxene is the liquidus phase for the two starting samples and clinopyroxene + liquid is the stable phase assemblage for a wide range of P-T-H_2O melt-fO_2 conditions. The VES9 charges (since no high pressure VS96-54A charge crystallized leucite and, therefore, the location of the leucite saturation curve in Figure 2 is estimated) demonstrate that leucite

comes second in the sequence, crystallizing under H_2O-poor concentrations (< 3 wt% H_2O in melt), consistent with the 0.1 MPa phase equilibria. For H_2O in melt > 3 wt%, phlogopite replaces leucite as the second phase of the sequence. The respective positions of the liquidus and phlogopite saturation curves (Fig. 2) suggest that clinopyroxene persists as the liquidus phase until H_2O-saturation (~ 6 wt% H_2O). Therefore, our data do not suggest the possibility that phlogopite can be stable on the liquidus (Esperança & Holloway, 1987; Righter & Carmichael, 1996). Finally, olivine occurred as a stable phase in only one charge (#7-1, Table 3), and no olivine stability field can be delineated.

Composition of crystalline phases

Clinopyroxenes are calcic, with 45-52% Wo, 32-51% En and 4-16% Fs, and Mg# (calculated with total Fe as Fe^{2+}) of 66-93. They contain 1.68-8.43 wt% Al_2O_3, 0.33-1.34 wt% TiO_2 and 0-0.30 wt% Cr_2O_3 (Table 6). There is no systematic difference between cpx crystallized from either VS96-54A or VES9. Clinopyroxene chemistry strongly correlates with the amount of cpx crystals present in the charge: the higher the amount of cpx, the lower the En, and the higher the Fs and the Al_2O_3 and TiO_2 contents. Upon crystallization, atomic (at.) Al + Ti + Na increases at the expense of at. Ca + Fe + Mg in cpx and so the proportion of quadrilateral cpx components decreases. Clinopyroxenes coexisting with olivine (olivine-added charges) have the lowest at. Al + Ti + Na and the highest at. Ca + Fe + Mg. In detail, compositions of experimental clinopyroxenes divide into two groups (Fig. 3). In the fluid-absent charges, Wo increases along with increasing Al_2O_3 (trend 1, Fig. 3), whereas in both the 0.1 MPa and the fluid-present charges, Wo decreases with Al_2O_3 (trend 2, Fig. 3). This contrasted behaviour correlates with systematic differences in melt H_2O concentrations, higher in the fluid-absent than in the fluid-present and 0.1 MPa charges (see below). Natural clinopyroxenes from Vesuvius follow the H_2O-rich trend (Fig. 3). Clinopyroxene contains substantial amounts of at. Fe^{3+} (estimated from structural formulae), progressively increasing with at. Al + Ti + Fe + Na. However, no correlation appears between at. Fe^{3+} in cpx and experimental fO_2. The Fe-Mg clinopyroxene-liquid exchange coefficient (K_d^{Cpx-L}) calculated with total Fe as Fe^{2+} in both phases is 0.30 $\pm$ 0.11 (average of all cpx-bearing charges from this study, n = 46). If the most extreme values (fluid-present charges #15-1, #15-2, #15-4, #16-1, #16-2, Table 4; 0.1 MPa charges #5, #6 (VS96-54A), #8, Table 5) are filtered out, the average K_d^{Cpx-L} becomes 0.27 $\pm$ 0.06, in excellent agreement with experimental data for hydrous basaltic compositions (0.26-0.31, Sisson & Grove, 1993; 0.29 $\pm$ 0.08, Pichavant & Macdonald, 2007).

Olivine crystallized in charge #7-1 is $Fo_{85.5}$ and it contains 0.29 wt% CaO (Fig. 4; Table 6). In the olivine-added experiments, compositions of residual crystals divide into two groups. At 1150°C, olivines have homogeneous Fo and CaO contents (respectively 90.9-91.3 and 0.10-0.18 wt%), close to the San Carlos starting crystals (Fig. 4). The olivine-liquid Fe-Mg exchange coefficient (K_d^{Ol-L}) calculated by averaging the data for these 4 charges and charge #7-1 is 0.34 $\pm$ 0.05, in agreement with literature values for comparable experimental conditions and compositions (0.27-0.33, Sisson & Grove, 1993; 0.25-0.39, Righter & Carmichael, 1996; 0.32 $\pm$ 0.04, Pichavant & Macdonald, 2007). This K_d^{Ol-L} uses melt FeO contents calculated from glass compositions (Kress & Carmichael, 1991) for P, T and fO_2 specific of each charge (Tables 3-4). At 1200°C, residual olivines are chemically zoned in Fe, Mg and Ca. Deviations from the initial olivine composition are marked. Rims reach Fo of 94.1 and 97.7 and CaO of 0.24 and 0.31 wt% for #17-2 and #18-1 respectively (Fig. 4). Olivine rim in charge #17-2 yields a K_d^{Ol-L} of 0.35 whereas the K_d^{Ol-L} for charge #18-1 (0.13, Table 4) is clearly lower than the range of equilibrium values. It is worth noting that #18-1 is the most oxidized charge in our dataset and it is possible that the calibration of Kress & Carmichael (1991) does not perform well for low FeO_t, high Fe^{3+} / Fe^{2+} melts such as #18-1 (Table 6).

Leucite compositions were determined in 5 out of a total of 7 leucite-bearing charges. They are tightly grouped and close to the leucite end-member (Table 6). There is no clear dependence of leucite composition with the type of experiments: leucites in high pressure fluid-present (run #12, Table 4) and 0.1 MPa (Table 5) charges are compositionally identical. There is also no apparent dependence of leucite composition with the starting material.

Experimental phlogopites have Mg# (calculated with total Fe as Fe^{2+}) between 70 and 81, at. K/(K+Na) between 0.93 and 0.96 and TiO_2 contents between 2.35 and 3.23 wt% (Fig. 5). The F concentration in phlogopite from charge #4-1 is below detection. There is no marked difference between micas crystallized from VS96-54A or VES9. Phlogopite becomes more magnesian with increasing temperature. Al^{VI} (0.505-0.665, 22 O basis), which makes up 9-12% of octahedral cations, slightly decreases with increasing temperature. The TiO_2 partition coefficient between phlogopite and melt (wt% TiO_2 in phlogopite / wt% TiO_2 in glass, data in Table 6) decreases from 3.57-5.23 (1000°C) to 2.28-3.71 (1050°C). If the equation calibrated for lamprophyres is used (Righter & Carmichael, 1996), experimental phlogopites from this study have at. $Fe^{3+}/\Sigma Fe$ between 0.02 and 0.15 (Fe_2O_3 between 0.2 and 1.7 wt%), which leads to a phlogopite-liquid Fe-Mg exchange coefficient ($K_d^{Phlog-L}$) of 0.28 $\pm$ 0.05 for Vesuvius magmas.

Melt compositions

Compositions of experimental glasses are given in Table 6. Note that, for charges #4-2 and #4-3, glass compositions have been corrected to account for quench phlogopite crystallization (see above). This was done by increasing their glass K_2O concentration respectively to 6.61 (from 5.4) and 6.88 (from 5.26) wt% (Table 6).

Glasses follow well-defined compositional trends, identical for VS96-54A and VES9 charges. Upon progressive crystallization and considering MgO, CaO or CaO/Al_2O_3 as a differentiation index, K_2O and Al_2O_3 strongly increase (up to ~ 9 and ~ 20 wt% respectively) while MgO, CaO and CaO/Al_2O_3 decrease (down to < 2, < 6 wt% and ~ 0.3 respectively, Fig. 6). Compositions of residual melts follow the evolution of Vesuvius whole-rocks (Fig. 6). In the TAS plot, glass compositions cover most of the Vesuvius differentiation sequence, progressively evolving from trachybasalt, tephrite, phonotephrite to tephriphonolite and approaching the phonolite domain (Fig. 1b). The experimental trends do not depend on the phase assemblage (i.e., presence of leucite, phlogopite or olivine) and they reflect the progressive crystallization of cpx, the dominant mineral phase in our experimental charges. Glasses from the olivine-added charges extend the compositional trends toward higher MgO, on one hand, and lower K_2O and Al_2O_3, on the other hand (Fig. 6), consistent with partial dissolution of olivine in these experiments. Primitive glass inclusions from the 1637-1944 activity evolve along trends similar to whole-rocks and experimental glasses. However, they extend to MgO concentrations beyond the VS96-54A and VES9 (whole-rocks and glasses) data points, in a range that is only attained by glasses from the olivine-added charges (Fig. 6).

Volatile concentrations

Glass H_2O concentrations are detailed in Tables 3-4. There is a good match between the different analytical results for H_2O (e.g., fluid-absent glasses #3-1, #5-1, #5-2, #5-4; fluid-present glasses #17-2, #5-3).

H_2O concentrations in VS96-54A and VES9 charges overlap. The fluid-absent charges have glass H_2O concentrations between 2.2 and 6.0 wt% with a frequency maximum at 3-4 wt%. For the fluid-present charges, glass H_2O concentrations range from 0.7 to 4.2 wt% (frequency maximum at 1-2 wt%). Therefore, one major difference between the fluid-absent and fluid-present charges concerns their respective glass H_2O concentrations, systematically higher in the former than in the latter (see above, Fig. 3). Several fluid-absent charges have

aH_2O of 1 or close to unity (e.g., #7-1, Table 3) impying that an hydrous (CO_2-free) fluid phase should in fact be present.

Glass CO_2 concentrations in 3 near-liquidus (1150-1200°C) 200 MPa fluid-present charges range from 1302 to 1861 ppm (Table 4). These results are consistent with the CO_2 solubility determined at 200 MPa and 1200°C for VES9 (Fig. 7).

DISCUSSION

Validation of experimental results

Before discussing the evolution of primitive Vesuvius magmas, it is first necessary to test the applicability of our experimental results. This is done below by comparing our synthetic charges with the mineralogical and petrological characteristics of Vesuvius eruption products.

In our experiments, mineral phases, assemblages and compositions typical of Vesuvius magmas have been obtained. Clinopyroxene crystallized either alone or with leucite and phlogopite and also, but very rarely, with olivine. Clinopyroxene is by far the dominant mineral phase in our charges, in broad agreement with the modal composition of Vesuvius magmas, although leucite, as a product of groundmass crystallization, may exceed the cpx proportion in lavas (e.g., Trigila & De Benedetti, 1993). The typical Vesuvius cpx trend (increase of Wo with Al_2O_3) is experimentally reproduced for H_2O > 2 wt% in melt (Fig. 3; see also below and Fig. 8). In the same way, compositions of experimental and natural leucite and phlogopite are in excellent agreement (Table 6; Fig. 5). However, one important natural phase, plagioclase, is missing in our experimental products. Calcic (An_{50-90}) plagioclase occurs in low amounts in mafic rocks such as the 1906 tephras (< 1%, Santacroce et al., 1993; Table 2), but reaches proportions > 5% in more evolved compositions (Trigila & De Benedetti, 1993). Another difference between natural and experimental products concerns olivine. Although never very abundant (< 1-2%, Santacroce et al., 1993; Cioni et al., 1995; Trigila & De Benedetti, 1993), olivine is ubiquitous in Vesuvius products (Marianelli et al., 1995; 1999; 2005; Dallai et al., 2011). Natural olivines have a wide range of Fo contents, including a well-defined Fo-rich group (Fo_{86-91}, CaO = 0.2-0.5 wt%) as well as Fo-poor, CaO-rich compositions (Fig. 4). The single composition ($Fo_{85.5}$) that spontaneously crystallized in the VS96-54A charge is at the Fo-poor end of the main (Fo-rich) natural group. More Fo-rich crystals (Fo_{91-98}) occur in the olivine-added charges. Concerning experimental liquids, the chemical trends exhibited by whole-rocks and glass inclusions have been closely reproduced (Fig. 1b; 6) and so the experiments confirm a genetic relation between the various terms of

the Vesuvius differentiation sequence, from trachybasalt, tephrite to phonolite. We conclude that there is a close correspondance between experimental and natural phase assemblages and compositions. However, we also stress the existence of significant differences between synthetic and natural products, especially concerning (1) plagioclase and (2) olivine.

Conditions of plagioclase crystallization in Vesuvius magmas can be inferred from previous studies. In the high pressure experiments on phonotephrite V_1 (Fig. 1a), plagioclase crystallizes after cpx and leucite in the low temperature, very low melt H_2O content region (Dolfi & Trigila, 1978). At 0.1 MPa, it appears third in tephrites to phonotephrites (Trigila & De Benedetti, 1993). Plagioclase also crystallizes in Vesuvius phonolites (Scaillet et al., 2008). Therefore, plagioclase is typical of relatively evolved Vesuvius rocks, consistent with its modal distribution in eruption products. We attribute the absence of plagioclase in our experiments to the choice of starting products more primitive, and of conditions closer to the liquidus, than in previous studies. In any case, plagioclase plays no critical role in the early evolution of Vesuvius magmas (e.g., Santacroce et al., 1993).

The mismatch between olivine in synthetic and natural products is most certainly not an experimental artefact since a range of techniques, conditions and starting compositions have been explored, both in this and previous experimental studies on Vesuvius rocks. Olivine was found neither in phonotephrite V_1 at high pressure (Dolfi & Trigila, 1978) nor in tephrites-phonotephrites at 0.1 MPa (Trigila & De Benedetti, 1993). This phase is also lacking in experiments on Vesuvius phonolites (Scaillet et al., 2008). We suggest that the near-absence of olivine in our experimental charges (and its total absence in previous experimental studies on Vesuvius) reflects the lack of eruption products representative of primitive olivine-crystallizing magmas (e.g., Dallai et al., 2011). As previously emphasized, only glass inclusions approach compositions of Vesuvius primitive magmas (Fig. 6). The composition of olivine that would be at equilibrium with our starting rocks is $Fo_{89.5}$ for VS96-54A and Fo_{87} for VES9 (calculations performed at NNO+1, 1200°C, 200 MPa with $K_d^{ol\text{-}L} = 0.34$ and glass compositions from Table 6). This is slightly less Fo-rich than the main Vesuvius olivine group ($Fo_{90\text{-}91}$, Fig. 4; Table 2). We conclude that the rocks used in this study are not representative of the most primitive Vesuvius liquids. This implies that our experiments on VS96-54A and VES9 simulate a stage that is relatively advanced in the magmatic evolution.

Primitive Vesuvius magmatic liquids: composition and intensive variables

Conditions of the early evolution of Vesuvius magmas can be reconstructed from the olivine-added experiments. These have been performed at 200 MPa, both under fluid-absent and

fluid-present conditions, and with both VS96-54A and VES9 glass. Two types of phase assemblages, ol + liquid and ol + cpx + liquid, were obtained. Residual olivines in the 1150°C charges have Fo ranging from 90 to 91, in the range of the most Fo-rich natural crystals (Fig. 4). At 1200°C, olivine Fo contents exceed the natural range, a consequence of the elevated temperature and highly oxidizing fO_2 (Table 4). Clinopyroxenes coexisting with Fo_{90-91} olivines at 1150°C have Mg# (90-91), Wo (48-49%), Al_2O_3 ($\leq$ 2 wt%), TiO_2 (< 0.5 wt%) and Cr_2O_3 (up to 0.3 wt%) similar to diopsides in Vesuvius eruption products (Rosi & Santacroce, 1983; Santacroce et al., 1993; Cioni et al., 1998; Fulignati et al., 2000; 2004a; Marianelli et al., 1995; 2005; Dallai et al., 2011; Table 2; Fig. 3; 8). Therefore, the 1150°C 200 MPa olivine-added experiments closely approach the environment of crystallization of natural diopsides. The lack of spinel in our experiments is attributed to the low Cr concentrations of our starting materials (VS96-54A: ~ 200 ppm, Marianelli, personal communication; VES9: 147 ppm, this study).

The three 1150°C 200 MPa olivine + clinopyroxene-bearing charges define the composition of cotectic melts in the MgO vs. CaO space (Fig. 9a). Charge #7-1, which spontaneously crystallized olivine, provides a point on the 1100°C, 50 MPa olivine + clinopyroxene cotectic. As found in other studies (Pichavant et al., 2009), the effect of decreasing pressure is to slightly increase the CaO content of cotectic melts for a given MgO. Relative to the 200 MPa cotectic, both the VS96-54A and VES9 starting glasses plot in the cpx field (Fig. 9a), consistent with the phase relations determined in this study (cpx as the liquidus phase, Fig. 2). In comparison, the three glasses from the 1150 and 1200°C olivine-bearing charges define control lines that extend from each starting glass toward Fo-rich olivine (Fig. 9a). They progressively shift away from the 200 MPa cotectic, plotting in the olivine primary field. Glass inclusions range from an evolved (MgO = 4-5, CaO ~ 10 wt%) to a more primitive (MgO = 9-10, CaO = 12-13 wt%) end-member (Fig. 9b). Inclusions with the lowest MgO plot either on the extension of the 1150°C 200 MPa cotectic, or above it. The most primitive (MgO = 8-10 wt%) glasses depart from the cotectic region, plotting in the olivine primary field. Their distribution follows the trend for the olivine-only VES9 charges, suggesting that the most primitive glass inclusions correspond to liquids whose composition is controlled by olivine-liquid equilibrium. Indeed, these most primitive inclusions are trapped in olivine (Fig. 9b). We conclude that olivine (+/- Cr-spinel) is the first phase to crystallize in primitive Vesuvius liquids (e.g., Marianelli et al., 1995).

The P-T-melt H_2O-fO_2 conditions of primitive Vesuvius liquids can be constrained from our experimental results. For the crystallization of Fo_{90-91} olivines, temperatures between

1150 and 1200°C are inferred from the location of the glass data points (Fig. 9a) and the Fo contents of olivines in the olivine-added charges. For comparison, temperatures > 1200°C were proposed for the crystallization of olivine + Cr-spinel in 1906 magmas (Marianelli et al., 1995). Clinopyroxene would join olivine on the liquidus at ~ 1150°C from our experiments (at 1200-1130°C from glass inclusion homogeneization temperatures, Marianelli et al., 1995; Cioni et al., 1998). Concerning volatiles, glass H_2O and CO_2 concentrations in the olivine-added fluid-present experiments (2.9-4.2 wt% H_2O; 1300-1900 ppm CO_2, Table 4) are within the range analyzed in glass inclusions (1.5-4.5 wt% H_2O; 600-4500 ppm CO_2, Fig. 7). Inspection of Fig. 7 indicates trapping pressures for the glass inclusions from $\leq$ 200 to a maximum of 300 MPa. This is much shallower than initially estimated (300-620 MPa, Marianelli et al., 1999) using fluid-melt saturation models not necessarily calibrated for Vesuvius liquid compositions (Behrens et al., 2009; Lesne et al., 2011), and narrowing the range (200-400 MPa) proposed in later studies (Marianelli et al., 2005). Table 7 gives representative examples of primitive Vesuvius liquids. They are trachybasaltic with K_2O ~ 4.5-5.5 wt%, K_2O/Na_2O between 2.75 and 4, MgO = 8-9 wt%, Mg# between 75 and 80 and CaO/Al_2O_3 between 0.9 and 0.95. Their redox state is estimated at NNO+0.6 to +0.9 from olivine-liquid equilibrium (Fig. 10). This quite oxidizing fO_2 range is independently confirmed by the application of the olivine-spinel oxybarometer (Ballhaus et al., 1991). ΔNNO of +0.7-1.2 are obtained for the 1944, 1906 (Marianelli et al., 1995) and 1637-1944 products (Marianelli et al., 2005), in excellent agreement with values derived from olivine-liquid equilibrium (Fig. 10). A similar fO_2 range (ΔNNO of +0.4-0.9) is calculated from olivine and spinel in VS97-718 (Table 2, see also below).

Early magmatic evolution

From the foregoing discussion, the question arises as to the transition from the early olivine-crystallizing stage (i.e., ol is the liquidus phase), only documented by the presence of Fo-rich olivines, diopsides, Cr-spinels and primitive glass inclusions, to the later clinopyroxene-crystallizing stage (i.e., cpx is the liquidus phase) recorded by Vesuvius eruption products. This transition must take place at high temperatures (1100-1200°C) and early in the magmatic evolution, since primitive products such as VS96-54A and VES9 (with liquidus temperatures in the range above) have cpx as the liquidus phase (Fig. 2). It is worth emphasizing that the change in liquidus phase is accompanied by the disappearance of olivine from the crystallization sequence since phase diagrams for mafic Vesuvius products lack ol stability

fields (Fig. 2; Dolfi & Trigila, 1978; Trigila & De Benedetti, 1993). In the following sections, potential mechanisms able to explain this transition are discussed.

Phlogopite crystallization. For melt H_2O concentrations of 1.5-4.5 wt%, temperatures between 1150 and 1200°C and pressures of 200-300 MPa, Fo-rich olivine and diopsidic clinopyroxene are under cotectic relationships in primitive K-rich basaltic liquids (Barton & Hamilton, 1978; Esperança & Holloway, 1987; Righter & Carmichael, 1996; Melzer & Foley, 2000). Consequently, phase assemblages composed successively of olivine and, when the derivative liquid reaches the cotectic, of olivine + clinopyroxene, are expected, as observed in the olivine-added experiments. Therefore, upon decreasing temperature, Vesuvius magmas should show a progressive evolution from olivine to olivine-clinopyroxene ($\pm$ Cr-spinel) phenocryst assemblages (e.g., Marianelli et al., 1995; Fig. 9b). Later, leucite and plagioclase, depending on P-T-melt H_2O-fO_2, would join the phase assemblage, as observed in the evolved terms of the Vesuvius suite, but olivine and clinopyroxene should continue to crystallize until phlogopite appears in the crystallization sequence. Indeed, the phlogopite-forming reaction is a possible mechanism to explain the replacement of olivine as the liquidus phase and its disappearance from the crystallization sequence (Barton & Hamilton, 1978; Esperança & Holloway, 1987; Righter & Carmichael, 1996; Melzer & Foley, 2000). However, our experiments show that temperatures < 1100°C are required for phlogopite to crystallize, which is lower than considered above for the transition between the ol- and cpx-crystallizing stages. This temperature range is consistent with the observation that phlogopites in Vesuvius products have Mg# (Fig. 5) lower than that needed for equilibrium with Fo-rich olivine or diopside (taking into account our determined $K_d^{Phlog\text{-}L}$ and $K_d^{Ol\text{-}L}$). Thus, phlogopites at Vesuvius crystallize from relatively evolved liquids. We conclude that the phlogopite-forming reaction takes place at a stage more advanced in the differentiation course than the transition between the ol- and cpx-crystallizing stages.

CO_2 flushing. At Vesuvius, thermal production of CO_2 is the consequence of the interaction between magma and the carbonate basement. A CO_2-rich fluid phase is thought to flush through the magma, increasing the $\delta^{18}O$ of Fo-rich Ol and diopside crystals (Dallai et al., 2011). Thus, the possibility that this CO_2-rich fluid inhibits olivine crystallization needs to be explored. Indeed, the phase relations of basaltic magmas depend on the fluid composition (Holloway & Burnham, 1972). As a general mechanism, increasing the proportion of CO_2 in the fluid (as with CO_2 flushing) at constant pressure and fO_2 will expand the stability field of Ol (as well as of other anhydrous silicates such as Cpx) towards higher temperature, because aH_2O (and so the melt H_2O content) will be lowered (Feig et al., 2006; Pichavant et al., 2009).

The consequence will be to promote (and not to inhibit) the crystallization of Ol, and of other anhydrous silicates as well. We conclude that a mechanism of CO_2 flushing explains neither the removal of olivine from the liquidus nor its replacement by clinopyroxene as the liquidus phase.

Magma mixing. The absence of olivine stability fields in phase diagrams determined for mafic Vesuvius rocks (this study, Dolfi & Trigila, 1978; Trigila & De Benedetti, 1993) raises the possibility that it could be the consequence of the choice of experimental starting materials. Magma mixing, more precisely mixing between primitive and phonotephritic to tephriphonolitic differentiates, is a common process at Vesuvius (Santacroce et al., 1993; Cioni et al., 1995; Marianelli et al., 1999; 2005; Table 2). One clear indication for magma mixing is the coexistence in the same rock of a mixed population of phenocrysts, each representing different (primitive and evolved) stages in the differentiation course. This is observed in one of our starting products (VS96-54A, and also in VS97-718, see above). If a magmatic mixture involving primitive and evolved fractions along the same differentiation sequence (as for Vesuvius) is used as starting material, orders of crystallization and phase proportions will be likely modified compared to the primitive end-member magma. However, phases on or near the liquidus (ol, cpx) should stay the same (see Walker et al., 1979 for an illustration). The disappearance of ol from the crystallization sequence would remain unexplained unless the evolved fraction dominates the mixture, forcing temperature to drop to < 1100°C where phlogopite would have the possibility to crystallize (see above). However, phlogopite is rare to absent in our starting products (see also Marianelli et al., 1999). It is never very abundant in Vesuvius lavas (e.g., Santacroce et al., 1993; Trigila & De Benedetti, 1993). In clinopyroxenites, phlogopite occurs as a minor phase (Cundari, 1982) and it is concluded, therefore, that conditions leading to the crystallization of large amounts of phlogopite are not met at Vesuvius.

Crystal accumulation. In the same way, phenocryst accumulation would make the experimental starting composition unrepresentative of a liquid. At Vesuvius, selective accumulation of clinopyroxene and leucite is observed in 1906 and 1944 products (e.g., Santacroce et al., 1993; Marianelli et al., 1999). Compositions of 1637-1944 whole-rocks reflect clinopyroxene, leucite and plagioclase modal proportions (Trigila & De Benedetti, 1993). As previously mentioned, one of our starting rocks (VS96-54A) is probably cpx cumulative (Marianelli et al., 1999). However, the experimental results for VES9, which is clearly not cpx cumulative, are almost identical to VS96-54A. In addition, cpx accumulation would not explain the disappearance of olivine from crystallization sequences. The order of

phase appearance would be affected (i.e., cpx would crystallize before ol), but the near liquidus assemblage should stay identical (cpx, ol) because ol and cpx are under cotectic relationships in primitive Vesuvius liquids (see above, Fig. 9a). Therefore, despite the complexities of our starting materials, we conclude that our conclusions regarding liquidus phase equilibria and crystallization sequences are robust and applicable to Vesuvius magmas.

Carbonate assimilation

Although considered for long as unconventional, carbonate assimilation has been recently re-introduced as a petrogenetic mechanism both at Vesuvius (Iacono Marziano et al., 2008; 2009 and references therein; Dallai et al., 2011) and other Italian volcanic districts (Iacono Marziano et al., 2007; Freda et al., 2008; Gaeta et al., 2009). Carbonate assimilation by mafic magmas produces CO_2 gas. The generated CaO melt component, together with the SiO_2 melt component, reacts with the Mg_2SiO_4 olivine component to produce a $CaMgSi_2O_6$ clinopyroxene component (Gaeta et al., 2006; Iacono Marziano et al., 2008). Therefore, carbonate assimilation promotes reaction between melt and olivine to crystallize clinopyroxene. Details of this reaction have been experimentally simulated: at 1150°C, 200 MPa, and starting from a magma with both olivine and clinopyroxene as liquidus phases, progressive addition of $CaCO_3$ (from 0 to 15 wt%) leads to the disappearance of liquidus olivine (Iacono Marziano et al., 2008). Glasses from these experiments (Fig. 9a) define a compositional trend that extends from the near-cotectic region (two data points correspond to charges with residual olivine still present) to well within the cpx primary phase field (one point corresponds to a charge where olivine has totally disappeared). Therefore, carbonate assimilation has the potential to drive primitive Vesuvius magmatic liquids from the olivine into the cpx primary phase field. In this process, olivine crystals initially present in the magma are resorbed. In detail, the amount of ol consumed depends on the amount (and Ca/Mg) of the carbonate material being assimilated. We conclude that carbonate assimilation provides an explanation for many puzzling characteristics of Vesuvius mafic rocks, including the absence of products representative of early olivine-crystallizing magmas, the low abundance of olivine in tephrites and phonotephrites, the occurrence of cpx (and not ol) as the liquidus phase and the absence of ol from crystallization sequences. Carbonate assimilation most probably starts when ascending mantle-derived magmas encounter the base of the crustal carbonate sequence (Iacono Marziano et al., 2009, Dallai et al., 2011), which is inferred to lie at ~ 11 km depth beneath Vesuvius (Berrino et al., 1998; Pommier et al., 2010).

We stress that the main new argument presented in this paper for carbonate assimilation comes from phase equilibrium considerations, i.e., erupted products have cpx on their liquidus despite the evidence that their parental liquids crystallized initially olivine. The model is similar to the one proposed for Colli Albani, a volcanic district of the potassic Roman province also built on a thick carbonate substratum (Freda et al., 2008; Gaeta et al., 2009). The Colli Albani products have cpx on the liquidus (Iacono Marziano et al., 2007; Freda et al., 2008), yet they are also derived from primitive parental magmas that crystallize Fo-rich olivine, clinopyroxene and spinel (Freda et al., 2008; Conte et al., 2009; Gaeta et al., 2009). The whole-rock composition of a leucite basanite (B23) from Vulsini is given in Table 7 (see also Fig. 9b), showing the similarity between the potassic Roman province and Vesuvius. Rocks such as B23 carry olivine phenocrysts; they are considered representative of parental magmas at Vulsini (Conte et al., 2009). Their compositional and mineralogical characteristics are analogous to those inferred for Vesuvius parental magmas whose direct observation is impossible.

Implications for magma feeding systems

At Vesuvius, erupted magmas have a wide range of compositions (Fig. 1b). Several explanations have been proposed to account for this diversity, observed both within a single and between different eruptions. As shown by Iacono Marziano et al. (2008), a decrease of the whole-rock SiO_2 at increasing $Na_2O + K_2O$ (trend (I) in Fig. 11) is the geochemical signature expected for carbonate assimilation. Magma desilication is the consequence of the consumption of the melt SiO_2 component to form clinopyroxene (Iacono Marziano et al., 2008). In the recent period of activity, only the 1637-1944 whole-rocks show a slight decrease of SiO_2 at increasing $Na_2O + K_2O$ (Marianelli et al., 2005; Fig. 1b). In comparison, the 1906 and 1944 eruptions have SiO_2 either constant or slightly increasing with $Na_2O + K_2O$. This trend (II, Fig. 11) is the result of the combination of various processes, including mixing between primitive and more evolved magmas, accumulation or removal of clinopyroxene and leucite, crystal fractionation (Santacroce et al., 1993; Marianelli et al., 1999) and, we suggest, carbonate assimilation. Trend (III), whose strong increase in SiO_2 contrasts with the two others and implies a very minor role for carbonate assimilation, is illustrated by the Pompei eruption (AD 79, Fig. 1b). Since our experimental glasses (especially the most evolved) mimic this natural trend, we interpret trend (III) to be mainly controlled by cpx fractionation under closed-system conditions. Therefore, variations in the extent of carbonate assimilation between eruptions can be detected.

For a volcanic system emplaced on a carbonate substratum, the main factors controlling the extent of carbonate assimilation would be (1) the supply rate of fresh magma, (2) its composition, (3) the structure and aspect ratio of the feeding system and (4) the volume of stored magma. Primitive magmas would be the most exposed to carbonate interaction since high MgO, presence of olivine phenocrysts and high temperatures enhance the assimilation process (see Iacono Marziano et al., 2008). Mafic batches intruding as an array of dykes or cracks the base of the carbonate sequence would develop magma-carbonate interfaces to promote assimilation. Carbonate interaction would be maximized with multiple high aspect ratio intrusions of small volume (Fig. 11B). Conversely, for a large volume, low aspect ratio reservoir, less frequently recharged hence colder, magma-carbonate interaction would be more limited. Fresh magmas would intersect the reservoir and be consumed by mixing with the resident differentiates (Cioni et al., 1995; Fig. 11C). Interaction with carbonate wall-rocks would be prevented by a thick skarn shell if the reservoir is long-lived (Cioni et al., 1998; Fulignati et al., 2004a; b), and also by the low bulk MgO and low temperature of the resident magma (Iacono Marziano et al., 2008). The former case corresponds to systems that feed open-conduit eruptions such as during 1637-1944 and in 1906 and 1944. These small volume eruptions would be controlled by the episodic arrival at shallow levels (Scandone et al., 2008) of tephritic magma batches generated at 7-11 km following carbonate assimilation by primitive trachybasalts (Fig. 7; 11B). Products from those eruptions should be significantly influenced by carbonate assimilation. Whole-rock trends from negative to slightly positive in the TAS diagram would be expected, as indeed observed (Fig. 1; 13B). The latter case is illustrated by large "mature" magma chambers (Cioni et al., 1998) tapped by Plinian eruptions such as Pompei. Their products should be on the whole little affected by carbonate assimilation, consistent with the marked SiO_2 increase found in AD 79 rocks (Fig. 1b; 11C). So, a correlation between the extent of carbonate assimilation and type of feeding system is proposed. The level of carbonate assimilation (which can be estimated from the proportion of sedimentary CO_2 in the gas plume, Iacono Marziano et al., 2009) might carry information on the type of feeding system presently beneath Vesuvius (Scaillet et al., 2008).

Implications for potassic magmatism in central-southern Italy

The new data presented in this paper on primitive Vesuvius magmas make it possible to make comparisons with other potassic volcanic centers from central-southern Italy. In Vesuvius as in other centers, an early phase assemblage composed of olivine, Cr-spinel and diopside is found in the most mafic products. Mineral compositions (notably Fo $\geq$ 89-90 and Cr# > 40)

demonstrate a near-primary mantle origin for the magmas (Fig. 12a). Another common feature is the scarcity to total absence of eruption products representative of near-primary magmas, as previously discussed for Vesuvius. At Phlegrean Fields, another Campanian volcano, eruptions provide no sampling of the primitive feeding units whose characteristics are inferred from rare lava domes (Melluso et al., 2011), and also from the nearby Ischia (D'Antonio et al., 2013; Moretti et al., 2013) and Procida (Mormone et al., 2011) volcanic centers. At Colli Albani, in the Roman province, the most primitive compositions are already quite evolved (Freda et al., 2008; Gaeta et al., 2009 and see above). Exceptions occur (e.g., Vulsini, Conte et al., 2009) but, in most systems, the primitive mineral phase assemblages and compositions have little or no whole-rock counterpart. This has led to consider crystals from the primitive phase assemblage (e.g., Fo-rich olivines) as *xenocrysts* (see for example Dallai et al., 2011; Melluso et al., 2011; Moretti et al., 2013). Although technically justified (olivine is too Fo-rich for equilibrium with bulk rock), a more unifying model is favoured here which recognizes the primitive minerals as *parental phenocrysts* and interprets their crystallization as an early step in the magmatic evolution.

Compositions of Cr-spinel are plotted as a function of the Fo content of their olivine hosts (Fig. 12a) for primitive mineral assemblages from Campanian volcanoes (Vesuvius, Phlegrean Fields, Ischia, Procida). For Phlegrean Fields, mineral compositions from the Accademia Dome are used (Melluso et al., 2011) and, for Ischia and Procida, data from the Vateliero (D'Antonio et al., 2013) and Solchiaro eruptions (D'Antonio & Di Girolamo, 1994) respectively. Redox states (ΔNNO values) are calculated from the olivine-spinel oxybarometer (Ballhaus et al., 1991; Fig. 12b). ΔNNO values range between +0.2 to +1.5 and no large difference is apparent between the four volcanoes considered. In particular, there is no evidence for very oxidized magmas, as proposed for Ischia (ΔNNO up to $\geq$ +3, D'Antonio et al., 2013; Moretti et al., 2013). The Procida data have lower fO_2 than the three other systems because our Solchiaro database lacks Cr-spinel inclusions in Fo > 88 olivines.

In the Cr# vs. Fo plot (Fig. 12a), the Vesuvius trend is rooted in the mantle array (Arai, 1994a; b), thus underlining the primitive character of olivines and spinels which come from VS97-718 and from products of the 1637-1944 period. Comparing with the other Campanian systems, the Vesuvius spinels are distinctive, being more Cr-rich. Although mantle melting and magma generation in central-southern Italy involve complex mantle sources and several metasomatic agents, the Cr# of spinel is generally considered as an indicator of the peridotitic component (e.g., Conticelli et al., 2004; Nikogosian & van Bergen,

2010; Moretti et al., 2013). Therefore, the distinctive composition of spinels would imply different peridotitic components in the source of Vesuvius and of other Campanian magmas.

CONCLUSIONS

(1) Clinopyroxene is the liquidus phase for the two primitive VS96-54A and VES9 Vesuvius products. This conclusion does not depend on the experimental conditions (H_2O-bearing fluid-absent, H_2O- and CO_2-bearing fluid-present, 0.1 MPa volatile-free).

(2) Compositions of experimental and natural clinopyroxene, leucite and phlogopite are in excellent agreement. Chemical trends exhibited by whole-rocks and glass inclusions have been experimentally simulated. This underlines the vital role of clinopyroxene in controlling crystal fractionation of Vesuvius magmas and confirms a genetic relation between the various terms of the natural differentiation sequence.

(3) The absence of plagioclase in our experimental products is attributed to the primitive nature of the starting compositions, and to P-T-melt H_2O-fO_2 conditions closer to the liquidus than in previous experimental studies on Vesuvius products. Plagioclase plays no critical role in the early magmatic evolution. The near-absence of olivine in our experiments reflects the lack of rocks representative of really primitive magmas at Vesuvius. Experiments on VS96-54A and VES9 simulate a stage that is relatively late in the magmatic evolution.

(4) The olivine-added experiments can be used to reconstruct the early evolution of Vesuvius magmas. Comparison between glasses from these experiments and from inclusions show that the most primitive Vesuvius melts are trachybasalts (K_2O ~ 4.5-5.5 wt%, MgO = 8-9 wt%, Mg# = 75-80, CaO/Al_2O_3 = 0.9-0.95) similar to other potassic magmas from the Roman province. They crystallize Fo-rich olivine (90-91) on their liquidus between 1150 and 1200°C and from a maximum of 300 to $\leq$ 200 MPa. They contain 1.5-4.5 wt% H_2O and 600-4500 ppm CO_2 and are quite oxidized (from NNO+0.4 to NNO+1.2).

(5) The transition from an early olivine-crystallizing to a later clinopyroxene-crystallizing stage requires a specific mechanism during differentiation of the Vesuvius magmatic suite. Assimilation of carbonate wall-rocks by ascending primitive magmas satisfactorily explains that erupted rocks have cpx on their liquidus despite the evidence that their parental liquids crystallized initially olivine. Carbonate assimilation erases the memory of the early olivine-crystallizing stage in Vesuvius magmas.

(6) Carbonate assimilation is promoted for primitive magma batches of relatively small volumes. For longer-lived, large volume, less frequently recharged hence colder reservoirs, magma-carbonate interaction is limited. A correlation between the extent of

carbonate assimilation and type of feeding system is proposed, with potential implications for the monitoring of the deep-seated activity of the volcano.

(7) Primitive magmas from Vesuvius and other Campanian volcanoes do not show systematic differences in their redox states. In contrast, the Cr# of Vesuvius spinels is distinctive and implies different peridotitic components in the source of Vesuvius and of other Campanian magmas.

ACKNOWLEDGEMENTS

This study was supported by the 2004-2006 DPC-INGV project on Vesuvius. I. Arienzo, A. M. Conte, S. Conticelli, M. D'Antonio, P. Marianelli, L. Melluso, R. Moretti and M. Piochi who provided discussions, data and samples. Presentation of this work benefited from constructive reviews by M. Rutherford, M. Gaeta and anonymous.

REFERENCES

Albarède F. (1995). *Introduction to Geochemical Modeling*. Cambridge University Press, 543 p.

Arai, S. (1994a). Characterization of spinel peridotites by olivine-spinel compositional relationships: review and interpretation. *Chemical Geology* **113**, 191-204.

Arai, S. (1994b). Compositional variation of olivine-chromian spinel in Mg-rich magmas as a guide to their residual spinel peridotites. *Journal of Volcanology and Geothermal Research* **59**, 279-293.

Ballhaus, C., Berry, C. F. & Green, D. H. (1991) High pressure experimental calibration of the olivine-orthopyroxene-spinel oxygen geobarometer: implications for the oxidation state of the upper mantle. *Contribution to Mineralogy and Petrology* **108,** 82-92**.**

Barclay, J. & Carmichael, I. S. E. (2004). A hornblende basalt from Western Mexico: water-saturated phase relations constrain a pressure-temperature window of eruptibility. *Journal of Petrology* **45**, 485-506.

Barton, M. & Hamilton, D. L. (1978). Water-saturated melting relations to 5 kilobars of three Leucite Hills lavas. *Contribution to Mineralogy and Petrology* **66**, 41-49.

Behrens, H., Romano, C., Nowak, M., Holtz, F. & Dingwell, D. B. (1996). Near-infrared determination of water species in glasses of the system $MAlSi_3O_8$ (M = Li, Na, K): an interlaboratory study. *Chemical Geology* **128**, 41-63.

Behrens, H., Misiti, V., Freda, C., Vetere, F., Botcharnikov, R. E. & Scarlato, P. (2009). Solubility of H_2O and CO_2 in ultrapotassic melts at 1200 and 1250°C and pressures from 50 to 500 MPa. *American Mineralogist* **94**, 105-120.

Belkin, H. E., Kilburn, C. R. J. & De Vivo, B. (1993). Sampling and major-element chemistry of the recent (AD 1631-1944) Vesuvius activity. *Journal of Volcanology and Geothermal Research* **58**, 273-290.

Berrino, G., Corrado, G. & Riccardi, U. (1998). Sea gravity data in the Gulf of Naples: a contribution to delineating the structural pattern of the Vesuvian area. *Journal of Volcanology and Geothermal Research* **82**, 139-150.

Burnham, C.W. (1979) The importance of volatile constituents. In: Yoder, H. S., Jr., (ed) *The evolution of igneous rocks.* Princeton University Press, pp. 439-482.

Cioni, R. (2000). Volatile content and degassing processes in the AD 79 magma chamber at Vesuvius (Italy). *Contribution to Mineralogy and Petrology* **140**, 40-54.

Cioni, R., Civetta, L., Marianelli, P., Metrich, N., Santacroce, R. & Sbrana, A. (1995) Compositional layering and syn-eruptive mixing of a periodically refilled shallow magma chamber: the AD 79 plinian eruption of Vesuvius. *Journal of Petrology* **36**, 739-776.

Cioni, R., Marianelli, P. & Santacroce, R. (1998) Thermal and compositional evolution of the shallow magma chambers of Vesuvius: evidence from pyroxene phenocrysts and melt inclusions. *Journal of Geophysical Research* **103**, 18227-18294.

Conte, A. M., Dolfi, D., Gaeta, M., Misiti V., Mollo, S. & Perinelli, C. (2009). Experimental constraints on evolution of leucite-basanite magma at 1 and 10^{-4} GPa: implications for parental compositions of Roman high-potassium magmas. *European Journal of Mineralogy* **21**, 763-782.

Conticelli, S., Melluso, L., Perini, G., Avanzinelli, R. & Boari, E. (2004). Petrologic, geochemical and isotopic characteristics of potassic and ultrapotassic magmatism in central-southern Italy: inferences on its genesis and on the nature of mantle sources. *Periodico Mineralogia* **73**, 135-164.

Costa, F., Scaillet, B. & Pichavant, M. (2004). Petrological and experimental constraints on the pre-eruption conditions of Holocene dacite from Volcán San Pedro (36°S, Chilean Andes) and the importance of sulphur in silicic subduction-related magmas. *Journal of Petrology* **45**, 855-881.

Cundari, A. (1982). Petrology of clinopyroxenites ejecra from Somma-Vesuvius and their genetic implications. *Tschermak Mineralogisches und Petrographische Mitteilungen*, 30, 17-35.

Dallai, L., Cioni, R., Boschi, C. & D'Oriano, C. (2011). Carbonate-derived CO_2 purging magma at depth: influence on the eruptive activity of Somma-Vesuvius, Italy. *Earth and Planetary Science Letters* **310**, 84-95.

Devine, J. D., Gardner, J. E., Brack, H. P., Layne, G. D. & Rutherford, M. J. (1995). Comparison of microanalytical methods for estimating H_2O contents of volcanic glasses. *American Mineralogist* **80**, 319-328.

Di Carlo, I., Pichavant, M., Rotolo, S. G. & Scaillet, B. (2006). Experimental crystallization of a high-K arc basalt: the golden pumice, Stromboli volcano (Italy). *Journal of Petrology* **47**, 1317-1343.

Dixon, J. E., Stolper, E. M. & Holloway, J. R. (1995). An experimental study of water and carbon dioxide solubilities in mid-ocean ridge basaltic liquids. Part I: calibration and solubility models. *Journal of Petrology* **36**, 1607-1631.

Dolfi, D. & Trigila, R. (1978). The role of water in the 1944 Vesuvius eruption. *Contribution to Mineralogy and Petrology* **67**, 297-304.

D'Antonio, M. & Di Girolamo, P. (1994). Petrological and geochemical study of mafic shoshonitic volcanics from Procida-Vivara and Ventotene islands (Campanian region, south Italy). *Acta Vulcanologica* **5**, 69-80.

D'Antonio, M., Tonarini, S., Arienzo, I., Civetta, L., Dallai, L., Moretti, R., Orsi, G., Mariachiara, A. & Trecalli, A. (2013). Mantle and crustal processes in the magmatism of the Campania region: inferences from mineralogy, geochemistry, and Sr-Nd-O isotopes of young hybrid volcanics of the Ischia island (south Italy). *Contribution to Mineralogy and Petrology* 1**65**, 1173-1194.

Esperança, S. & Holloway, J. R. (1987). On the origin of some mica-lamprophyres: experimental evidence from a mafic minette. *Contribution to Mineralogy and Petrology* **95**, 207-216.

Feig, S. T., Koepke, J. & Snow, J. E. (2006). Effect of water on tholeiitic basalt phase equilibria: an experimental study under oxidizing conditions. *Contribution to Mineralogy and Petrology* **152**, 611-638.

Freda, C., Gaeta, M., Misiti, V., Mollo, S., Dolfi, D & Scarlato, P. (2008). Magma-carbonate interaction: an experimental study on ultrapotassic rocks from Alban Hills (Central Italy). *Lithos* **101**, 397-415.

Fulignati, P., Marianelli, P. & Sbrana A. (2000). The feeding system of the 1944 eruption of Vesuvius: melt inclusion data from dunitic nodules. *Neues Jahrbuch für Mineralogie – Monatshefte* **9**, 419-432.

Fulignati, P., Marianelli, P., Santacroce, R. & Sbrana A. (2004a). Probing the Vesuvius magma chamber-host rock interface through xenoliths. *Geological Magazine* **141**, 417-428.

Fulignati, P., Marianelli, P., Métrich, N., Santacroce, R. & Sbrana A. (2004b). Towards a reconstruction of the magmatic feeding system of the 1944 eruption of Mt Vesuvius. *Journal of Volcanology and Geothermal Research* **133**, 13-22.

Gaeta, M., Freda, C., Christensen, J. N., Dallai, L., Marra, F., Karner, D. B. & Scarlato, P. (2006). Time-dependent geochemistry of clinopyroxene from the Alban Hills (Central Italy): clues to the source and evolution of ultrapotassic magmas. *Lithos* **86**, 330-346.

Gaeta, M., Di Rocco, T. & Freda, C. (2009). Carbonate assimilation in open magmatic systems: the role of melt-bearing skarns and cumulate-forming processes. *Journal of Petrology* **50**, 361-385.

Holloway, J. R. (1987). Igneous fluids. In: Eugster, H. P. & Carmichael, I. S. E. (eds) *Thermodynamic Modeling of Geological Materials: Minerals, Fluids and Melts. Mineralogical Society of America, Reviews in Mineralogy* **17**, 211-233.

Holloway, J. R. & Burnham, C. W. (1972). Melting relations of basalt with equilibrium water pressure less than total pressure. *Journal of Petrology* **13**, 1–29

Iacono Marziano, G., Gaillard, F. & Pichavant, M. (2007). Limestone assimilation and the origin of CO_2 emissions at the Alban Hills (Central Italy): constraints from experimental petrology. *Journal of Volcanology and Geothermal Research* **166**, 91-105.

Iacono Marziano, G., Gaillard, F. & Pichavant, M. (2008). Limestone assimilation by basaltic magmas: an experimental re-assessment and application to Italian volcanoes. *Contribution to Mineralogy and Petrology*, **155**, 719-738.

Iacono Marziano, G., Gaillard, F., Scaillet, B., Pichavant, M. & Chiodini, G. (2009). Role of non-mantle CO_2 in the dynamics of volcano degassing: the Mount Vesuvius example. *Geology* **37**, 319-322.

Iacono Marziano, G., Morizet , Y., Le Trong, E. & Gaillard, F. (2012). New experimental data and semi-empirical parameterization of H_2O–CO_2 solubility in mafic melts. *Geochimica et Cosmochimica Acta* 97, 1-23.

Kress, V. C. & Carmichael, I. S. E. (1991). The compressibility of silicate liquids containing Fe_2O_3 and the effect of composition, temperature, oxygen fugacity and pressure on their redox states. *Contribution to Mineralogy and Petrology* **108**, 82-92.

Lesne, P., Scaillet, B., Pichavant, M. & Bény, J.-M. (2011). The carbon dioxide solubility in alkali basalts: an experimental study. *Contribution to Mineralogy and Petrology* **162**, 153-168.

Marianelli, P., Metrich, N., Santacroce, R. & Sbrana, A. (1995) Mafic magma batches at Vesuvius: a glass inclusion approach to the modalities of feeding stratovolcanoes. *Contribution to Mineralogy and Petrology* **120**, 159-169.

Marianelli, P., Metrich, N. & Sbrana, A. (1999). Shallow and deep reservoirs involved in magma supply of the 1944 eruption of Vesuvius. *Bulletin of Volcanology* **61**, 48-63.

Marianelli, P., Sbrana, A., Metrich, N. & Cechetti, A. (2005). The deep feeding system of Vesuvius involved in recent violent strombolian eruptions. *Geophysical Research Letters* **32**, L2306.

Martel, C., Pichavant, M., Holtz, F., Scaillet, B., Bourdier, J.-L. & Traineau, H. (1999). Effects of fO_2 and H_2O on andesite phase relations between 2 and 4 kbar. *Journal of Geophysical Research* **104**, 29453-29470.

Melluso, L., De' Gennaro, R., Fedele, L., Franciosi, L. & Morra, V. (2011). Evidence of crystallization in residual, Cl-F-rich, agpaïtic, trachyphonolitic magmas and primitive Mg-rich basalt-trachyphonolite interaction in the lava domes of the Phlegrean Fields (Italy). *Geological Magazine* **49**, 532-550.

Melzer, S. & Foley, S. F. (2000). Phase relations and fractionation sequences in potassic magma series modelled in the system $CaMgSi_2O_6$ – $KAlSiO_4$ – Mg_2SiO_4 – SiO_2 –F_2O_{-1} at 1 bar to 18 kbar. *Contributions to Mineralogy and Petrology* **138**, 186-197.

Mormone, A., Piochi, M., Bellatrecia, F., De Astis, G., Moretti, R., Della Ventura G., Cavallo, A. & Mangiacapra, A. (2011). A CO_2-rich magma source beneath the Phlegrean volcanic district (southern Italy): evidence from a melt inclusion study. *Chemical Geology* **287**, 66-80.

Moretti, R., Arienzo, I., Orsi, G., Civetta, L. & D'Antonio, M. (2013). The deep plumbing system of Ischia: a physico-chemical window on the fluid-saturated and CO_2-sustained Neapolitan volcanism (southern Italy). *Journal of Petrology* **54**, 951-984.

Nikogosian, I. K. & van Bergen, M. J. (2010). Heterogeneous mantle sources of potassium-rich magmas in central-southern Italy: melt inclusion evidence from Roccamonfina and Ernici (Mid Latina Valley). *Journal of Volcanology and Geothermal Research* **197**, 279-302.

Pichavant, M. & Macdonald, R. (2007). Crystallization of primitive basaltic magmas at crustal pressures and genesis of the calc-alkaline igneous suite: experimental evidence from St Vincent, Lesser Antilles arc. *Contributions to Mineralogy and Petrology* **154**, 535-558.

Pichavant, M., Di Carlo, I., Le Gac, Y., Rotolo, S. & Scaillet, B. (2009). Experimental constraints on the deep magma feeding system at Stromboli volcano, Italy. *Journal of Petrology* **50**, 601-624.

Pommier, A., Tarits, P., Hautot, S., Pichavant, M., Scaillet, B. & Gaillard, F. (2010). A new petrological and geophysical investigation of the present-day plumbing system of Mount Vesuvius. *Geochemistry, Geophysics, Geosystems* **11**, 10.1029/2010GC003059.

Pownceby, M. I. & O'Neill, H. St. C. (1994). Thermodynamic data from redox reactions at high temperatures. III. Activity-composition relations in Ni-Pd alloys from EMF measurements at 850-1250 K and calibration of the NiO + Ni-Pd assemblage as a redox sensor. *Contributions to Mineralogy and Petrology* **116**, 327-339.

Richet, P., Whittington, A., Holtz, F., Behrens, H., Ohlhorst, S. & Wilke, M. (2000). Water and the density of silicate glasses. *Contributions to Mineralogy and Petrology* **138**, 337-347.

Righter, K & Carmichael, I. S. E. (1996). Phase equilibria of phlogopite lamprophyres from western Mexico: biotite liquid equilibria and P-T estimates for biotite-bearing igneous rocks. *Contribution to Mineralogy and Petrology* 123, 1-21.

Robie, R. A., Hemingway, B. S. & Fisher, J. R. (1979). Thermodynamic properties of minerals and related substances at 298.15 K and 1 bar (10^5 pascals) pressure and at higher temperatures. *US Geological Survey Bulletin* **1452**.

Rolandi, G., Munno, R. & Postiglione, I. (2004) The A.D. 472 eruption of the Somma volcano. *Journal of Volcanology and Geothermal Research* **129**, 291-319.

Rosi, M. & Santacroce, R. (1983) The A.D. 72 "Pollena" eruption: volcanological and petrological data for this poorly-known, plinian-type event at Vesuvius. *Journal of Volcanology and Geothermal Research* **17**, 249-271.

Rosi, M., Principe, C. & Vecci, R. (1993) The 1631 Vesuvius eruption. A reconstruction based on historical and stratigraphical data. *Journal of Volcanology and Geothermal Research* **58**, 151-182.

Santacroce, R., Bertagnini, A., Civetta, L., Landi, P. & Sbrana, A. (1993) Eruptive dynamics and petrogenetic processes in a very shallow magma reservoir: the 1906 eruption of Vesuvius. *Journal of Petrology* **34**, 383-425.

Scaillet, B. & Evans, B. W. (1999). The 15 June 1991 eruptionof Mount Pinatubo. I. Phase equilibria and pre-eruption P-T-fO_2-fH_2O conditions of the dacite magma. *Journal of Petrology* **40**, 381-411.

Scaillet, B., Pichavant, M., Roux, J., Humbert, G. & Lefèvre, A. (1992). Improvements of the Shaw membrane technique for measurements and control of fH_2 at high temperatures and pressures. *American Mineralogist* **77**, 647-655.

Scaillet, B., Pichavant, M., & Roux, J. (1995). Experimental crystallization of leucogranite magmas. *Journal of Petrology* **36**, 663-705.

Scaillet, B., Pichavant, M. & Cioni, R. (2008). Upward migration of Vesuvius magma chamber over the past 20,000 years. *Nature* **455**, 216-220.

Scandone, R., Giacomelli, L. & Speranza, F. (2008). Persistent activity and violent strombolian eruptions at Vesuvius between 1631 and 1944. *Journal of Volcanology and Geothermal Research* **170**, 167-180.

Sisson, T. W. & Grove, T. L. (1993). Experimental investigation of the role of H_2O in calc-alkaline differentiation and subduction zone magmatism. *Contributions to Mineralogy and Petrology* **113**, 143-166.

Taylor, J. R., Wall, V. J. & Pownceby, M. I. (1992). The calibration and application of accurate redox sensors. *American Mineralogist* **77**, 284-295.

Trigila, R. & De Benedetti, A. A. (1993) Petrogenesis of Vesuvius historical lavas constrained by Pearce element ratios analysis and experimental phase equilibria. *Journal of Volcanology and Geothermal Research* **58**, 315-343.

Villemant, B., Trigila, R. & De Vivo, B. (1993). Geochemistry of Vesuvius volcanics during 1631-1944 period. *Journal of Volcanology and Geothermal Research* **58**, 291-313.

Walker, D., Shibata, T. & DeLong, S. E. (1979). Abyssal tholeiites from the Oceanographer fracture zone. Part II. Phase equilibria and mixing. *Contribution to Mineralogy and Petrology* **70**, 111-125.

Wallace, P. & Carmichael, I. S. E. (1989). Minette lavas and associated leucitites from the western front of the Mexican volcanic belt: petrology, chemistry and origin. *Contribution to Mineralogy and Petrology* **103**, 470-492.

FIGURE CAPTIONS

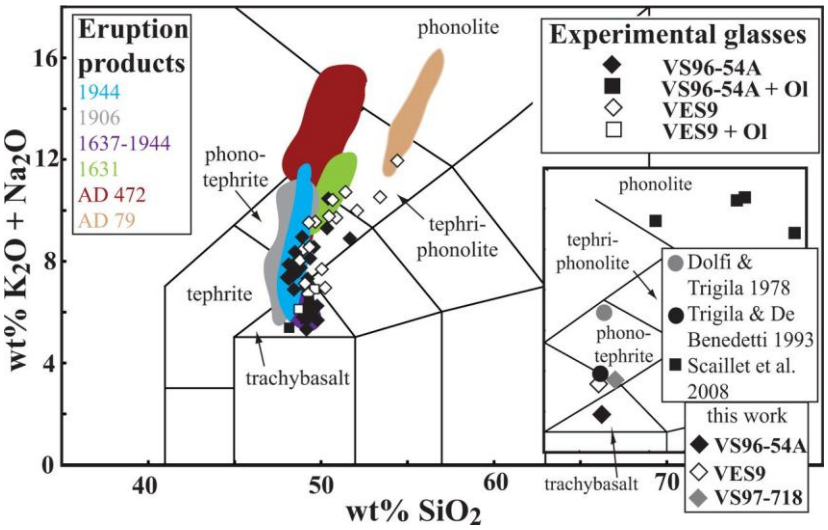

Fig. 1. Total alkali – silica (TAS) diagram for Vesuvius starting materials, experimental glasses and eruption products. (a) Insert shows composition of starting materials. Rocks considered in this study are a trachybasalt (VS96-54A) and two tephrites (VES9, VS97-718). Note the similarity between tephrites from this study and the V36 composition of Trigila & De Benedetti (1993). The composition of the phonotephrite V_1 of Dolfi & Trigila (1978) is indicated. The four phonolites studied by Scaillet et al. (2008) are also shown. (b) Comparison between experimental glasses (this study) and Vesuvius eruption products. The experimental data points are distinguished by starting material (either VS96-54A or VES9). Glasses from the olivine-added experiments are plotted with a different symbol. Whole-rock compositions for the 79 AD (Pompei), 472 AD (Pollena), 1631, 1637-1944 period, 1906 and 1944 eruptions from Rosi & Santacroce (1983), Rosi et al. (1993), Santacroce et al. (1993), Cioni et al. (1995; 1998) and Marianelli et al. (1999; 2005).

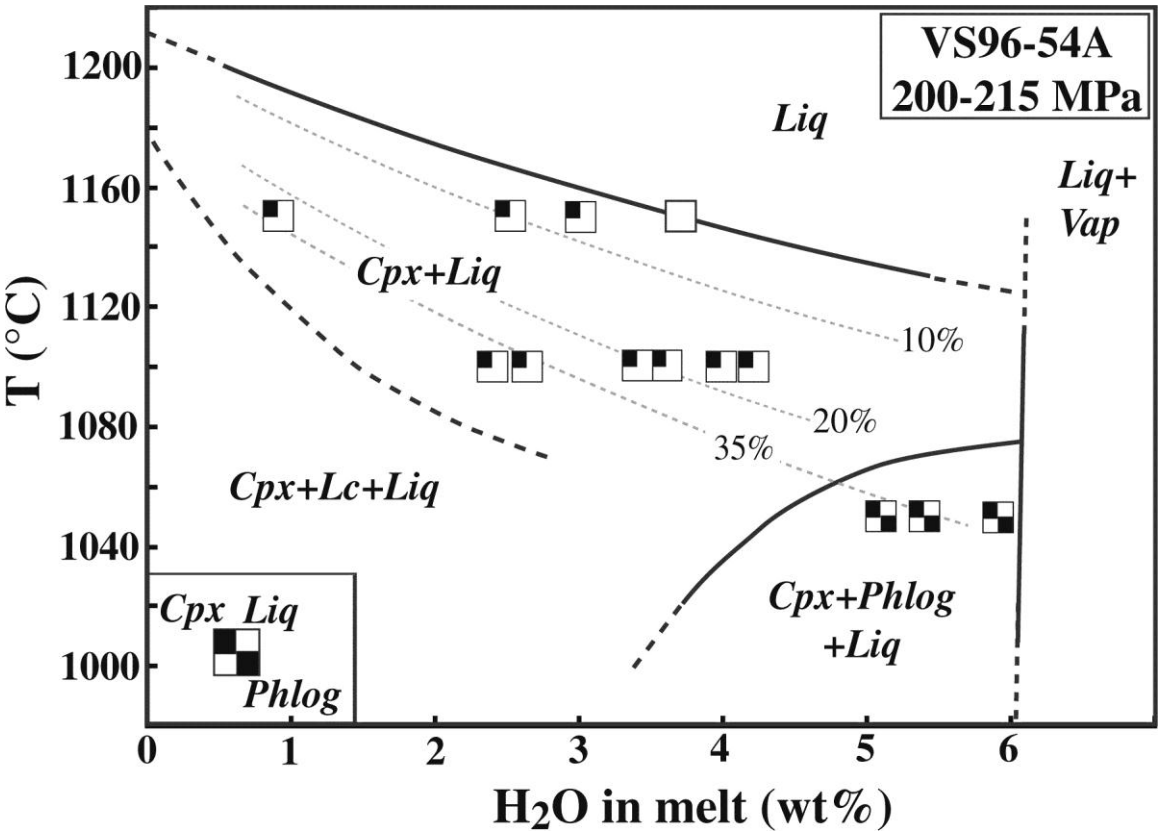

Fig. 2. T-H_2O in melt phase diagram for VS96-54A showing experimental data points (squares), saturation curves (dashed when estimated), phase assemblages and stability fields. The diagram combines experimental results from fluid-absent (#1, 2, 3, 4, Table 3) and fluid-present experiments (#13, Table 4). Total pressures range between 200 and 215 MPa. Redox conditions range between NNO+0.5 and +1.5 except for run #2 (1100°C) which is more oxidized (Tables 3, 4). Thin dotted lines are contours of clinopyroxene proportions (in wt%) constructed excluding data from the oxidized run #2 charges. Liq: liquid (silicate melt); Cpx: clinopyroxene; Phlog: phlogopite; Lc: leucite; Vap: vapour phase. Note that, in the diagram, the vapour is a H_2O-rich, CO_2-free, phase and so charge #13-1 (which contains a CO_2-rich fluid) lies outside the Liq+Vap field.

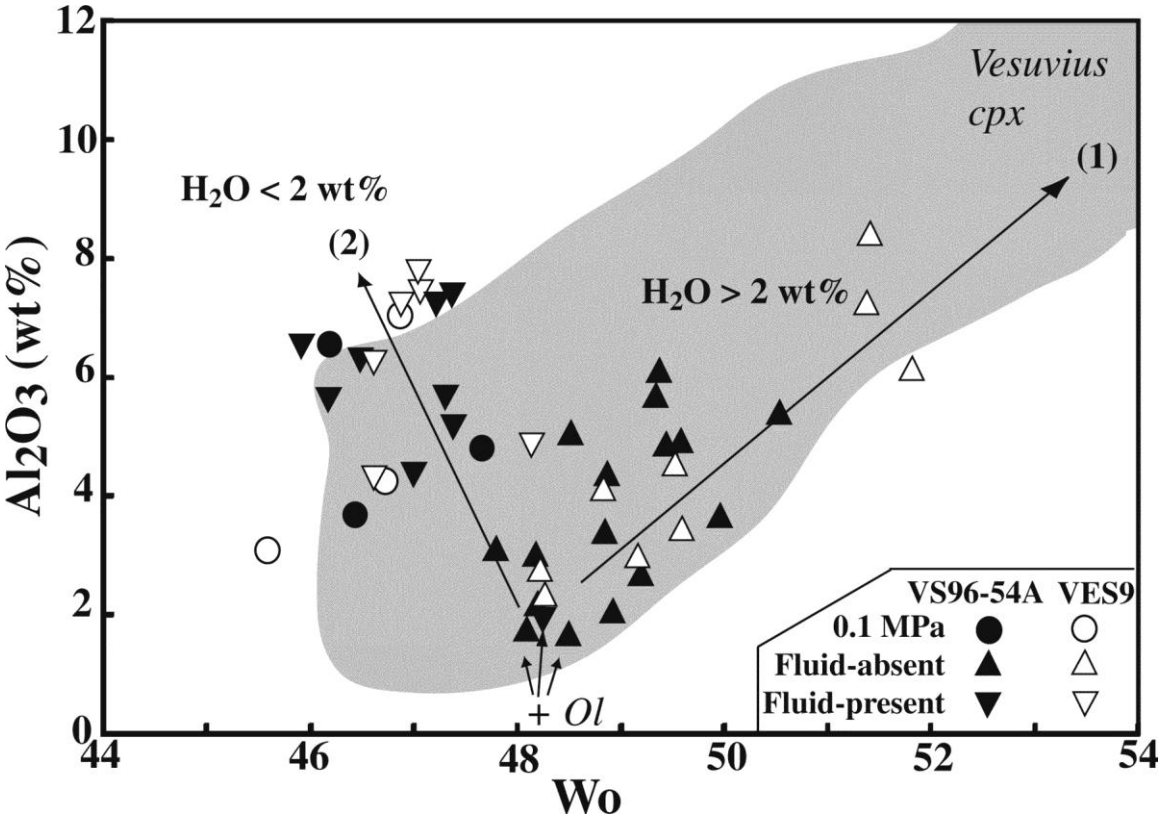

Fig 3. Al_2O_3 vs. Wo (calculated with total Fe as Fe^{2+}) for experimental clinopyroxenes of this study (Table 6). The data points are distinguished by type of experiment (0.1 MPa, fluid-absent, fluid-present), starting material (either VS96-54A or VES9) and addition of olivine (+ Ol). See Tables 3-5 for the detail of experimental conditions. The grouping of the fluid-absent H_2O-rich (H_2O in melt > 2 wt%) experimental data points defines a positive correlation between wt% Al_2O_3 and Wo (trend (1) indicated by an arrow). In contrast, both the 0.1 MPa and fluid-present (H_2O in melt < 2 wt%) experimental data define a negative Al_2O_3 - Wo correlation (trend (2) indicated by an arrow). Clinopyroxenes from the 3 olivine-added charges have the lowest Al_2O_3 contents of the experimental dataset. The grey field marks the compositional domain for natural Vesuvius clinopyroxenes (both phenocrysts in lavas and cumulus phases in clinopyroxenite nodules). For the natural clinopyroxenes, data from Rosi & Santacroce (1983), Santacroce et al. (1993), Trigila & De Benedetti (1993), Cioni et al. (1995; 1998), Marianelli et al. (1995; 1999; 2005), Cioni (2000), Fulignati et al. (2000; 2004a), Rolandi et al. (2004), Dallai et al. (2011) and this study (Table 2).

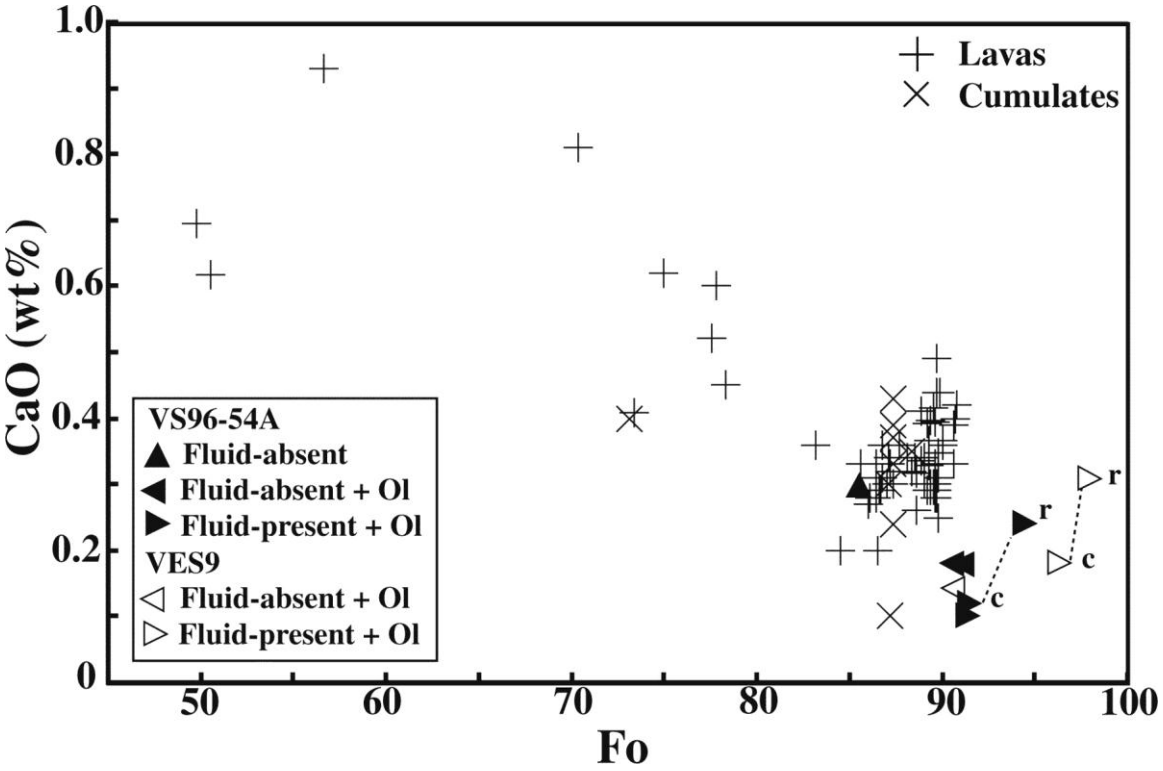

Fig. 4. CaO vs. Fo for experimental olivines of this study and comparison with olivine composition in Vesuvius lavas and cumulates. Experimental data in Table 6. Natural compositions (both phenocrysts in lavas and cumulus phases in dunitic nodules) from Trigila & De Benedetti (1993), Cioni et al. (1995), Marianelli et al. (1995; 1999; 2005), Fulignati et al. (2000), Dallai et al. (2011) and this study (Table 2). The data points are distinguished by type of experiment (either fluid-absent or fluid-present), starting material (either VS96-54A or VES9) and addition of olivine. See Tables 3-5 for the detail of experimental conditions. For the chemically zoned olivines of the olivine-added charges #17-2 and #18-1, two data points are plotted, one for the core (labelled c) and the other for the rim (labelled r). Core and rim compositions are connected by dashed lines.

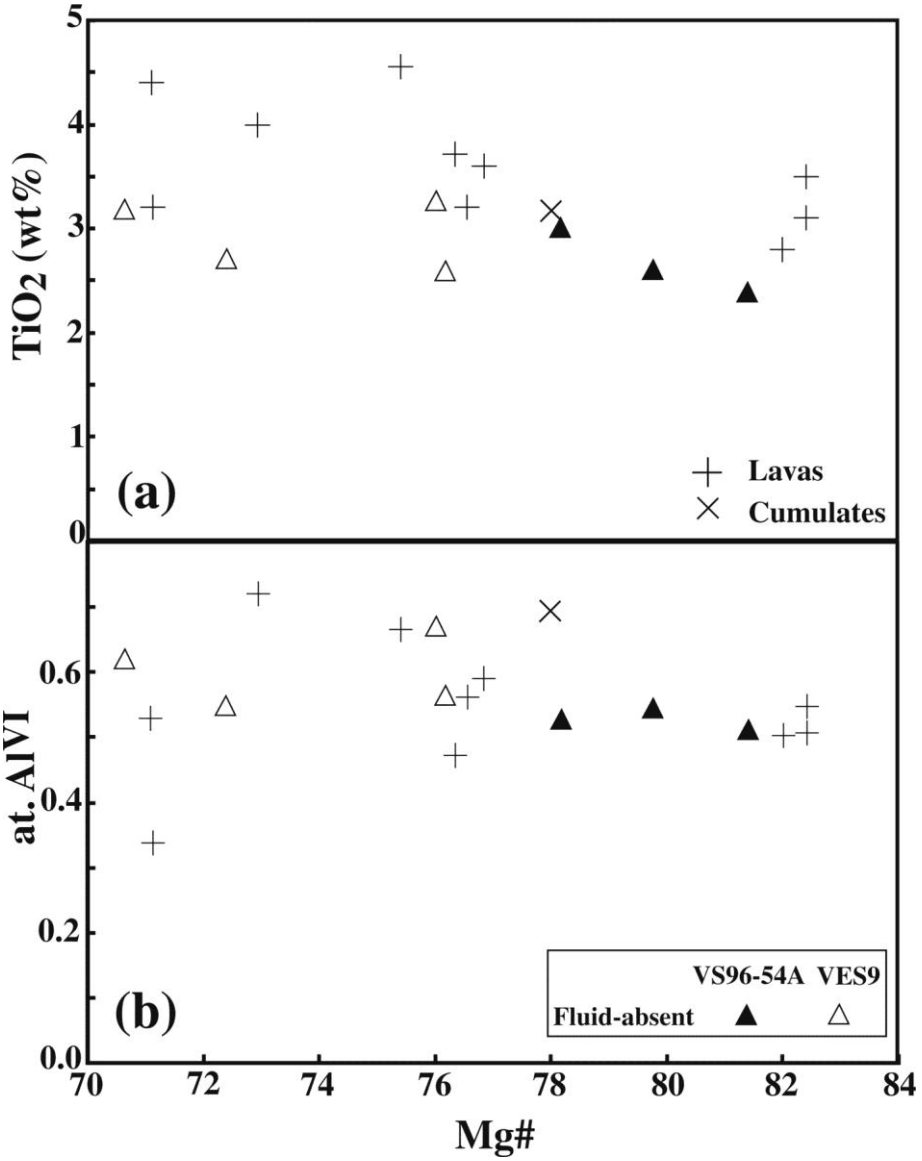

Fig. 5. (a) TiO_2 and (b) at. Al^{VI} (calculated on a 22 O basis) vs. Mg# (calculated with total Fe as Fe^{2+}) for experimental phlogopites of this study, and comparison with phlogopite composition in Vesuvius products. Experimental data in Table 6. For the lavas, data are from Rosi & Santacroce (1983), Cioni et al. (1995), Marianelli et al. (2005), Rolandi et al. (2004) and, for the cumulates (clinopyroxenites), from Cundari (1982). All the data points correspond to fluid-absent experiments and they are distinguished by starting material (either VS96-54A or VES9). See Tables 3-5 for the detail of experimental conditions.

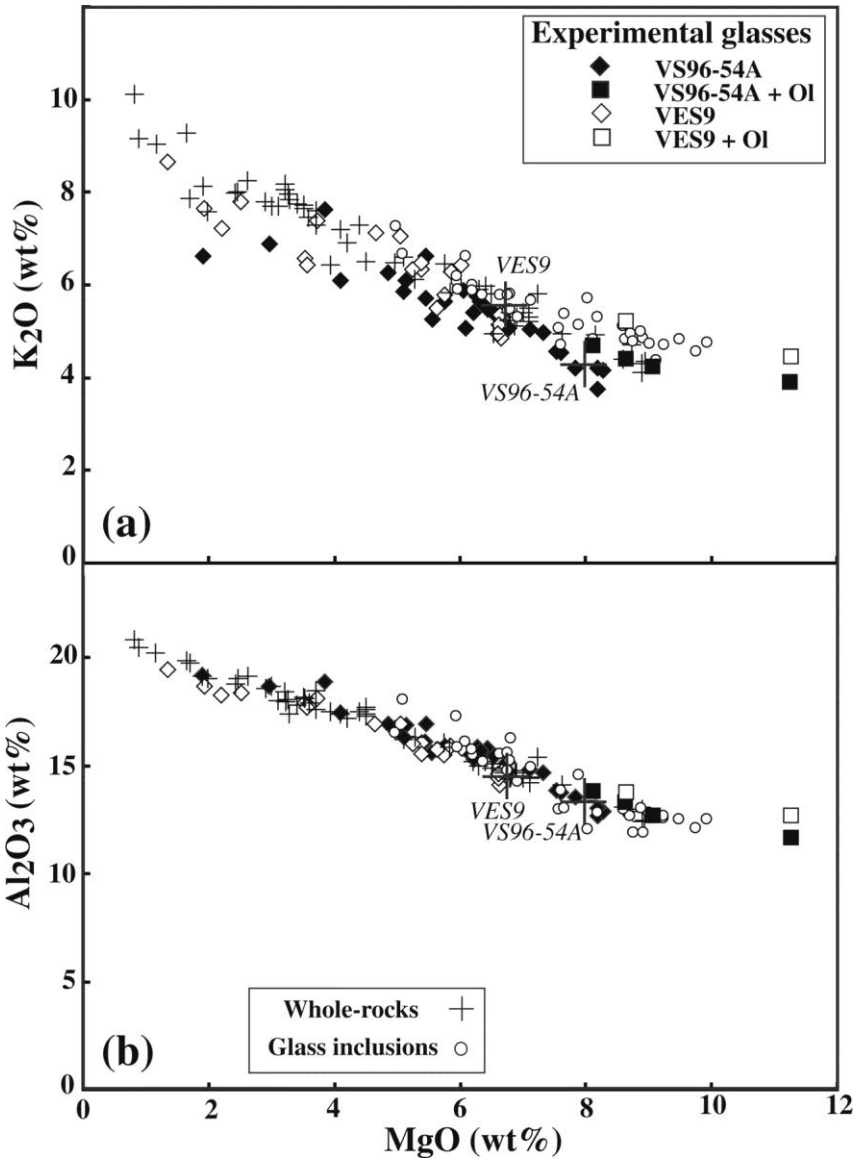

Fig. 6. MgO variations diagrams for experimental glasses from this study and comparison with selected natural compositions from Vesuvius (whole-rocks and glass inclusions). (a) K_2O vs. MgO. (b) Al_2O_3 vs MgO. Data for the experimental glasses in Table 6. Whole-rock data for the 472 AD, 1631, 1637-1944, 1906 and 1944 eruptions from Rosi & Santacroce (1983), Rosi et al. (1993), Santacroce et al. (1993), Cioni et al. (1998) and Marianelli et al. (1999; 2005). The glass inclusions are for the 1637-1944 period of activity (recalculated compositions from Marianelli et al., 1995; 1999; 2005). The experimental data points are distinguished by starting material (either VS96-54A or VES9). Glasses from the olivine-added experiments are plotted with a different symbol. See Tables 3-5 for the detail of experimental conditions. For clarity, the whole-rock analyses (Table 1) of VS96-54A (Marianelli et al., 1999) and VES9 (this study, Table 1) are plotted with a larger symbol.

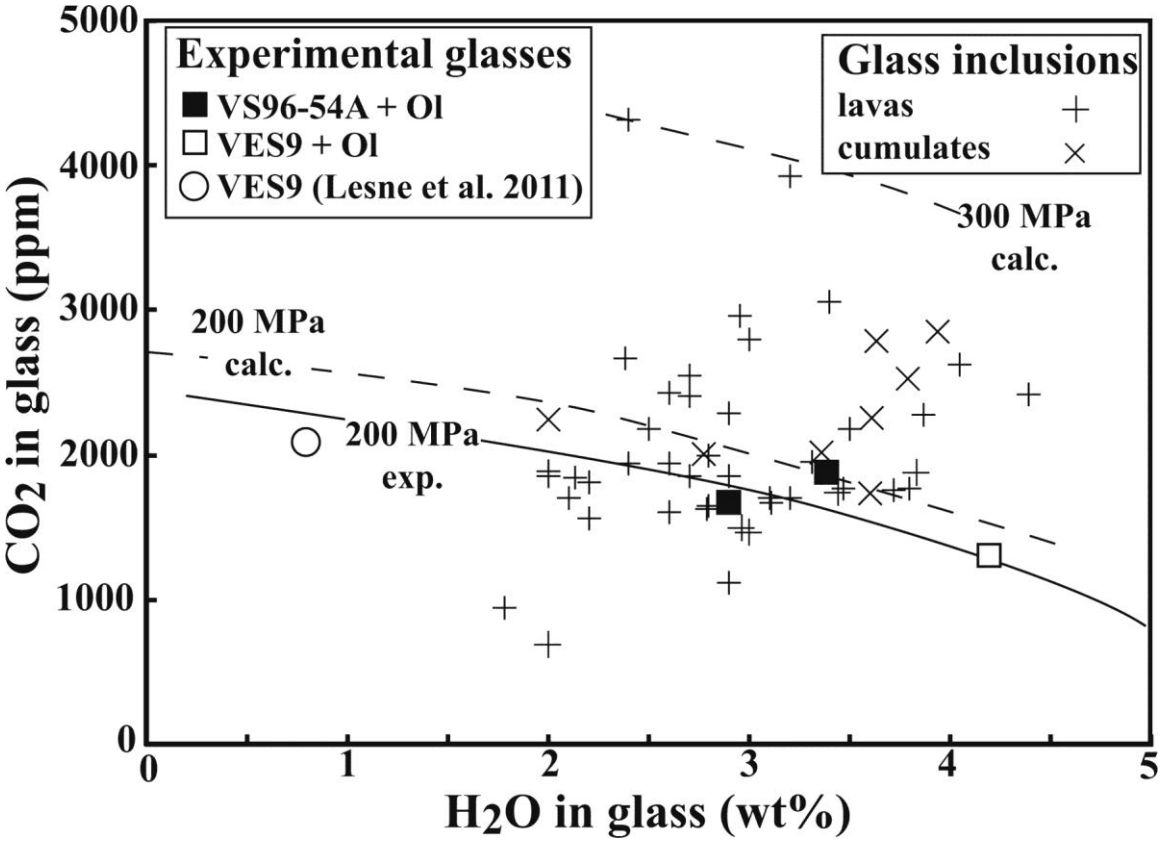

Fig. 7. H_2O and CO_2 concentrations of experimental glasses and of glass inclusions. The experimental data plotted are from this study (1150 and 1200°C 200 MPa fluid-present olivine-added charges, Table 4) and from Lesne et al. (2011), the latter being a CO_2 solubility measurement for VES9 melt at 1200°C, 200 MPa. Experimental data points from this study are distinguished by starting material (either VS96-54A or VES9). The experimental results collectively define the concentration of H_2O and CO_2 in primitive Vesuvius melts at equilibrium with H_2O-CO_2 fluids for a pressure of 200 MPa. The solid curve is the 200 MPa isobar drawn from the experimental datapoints. The dashed curves are 200 and 300 MPa fluid-melt saturation isobars calculated with the model of Iacono Marziano et al. (2012). The glass inclusions include data for the AD 79, 1794, 1822, 1872, 1906 and 1944 products (recalculated compositions from Marianelli et al., 1995; 1999; 2005, inclusions mostly trapped in olivine and more rarely in clinopyroxene, and from Cioni et al., 2000, inclusions in clinopyroxene) and for cumulates (dunitic nodules, Fulignati et al., 2000, inclusions trapped in olivine).

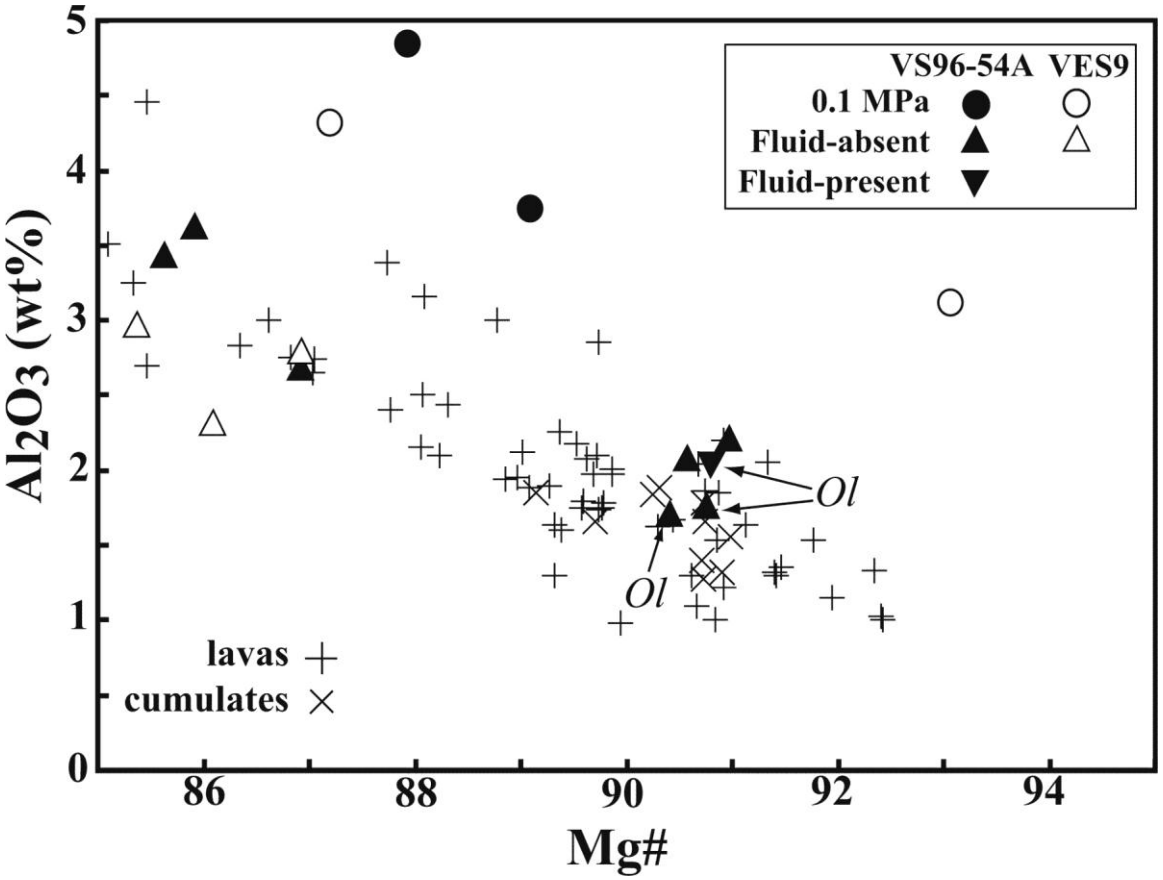

Fig. 8. Comparison between compositions of diopsidic (Mg# > 85) clinopyroxenes in Vesuvius lavas and cumulates and in experiments. Mg# in clinopyroxene is calculated with total Fe = FeO. Data for experimental clinopyroxenes in Table 6. For natural clinopyroxenes, source of data as in Fig. 3. The experimental data points are distinguished by type of experiment (0.1 MPa, fluid-absent, fluid-present), starting material (either VS96-54A or VES9) and addition of olivine (Ol). See Tables 3-5 for the detail of experimental conditions. Crystals from fluid-absent and fluid-present charges plot along the natural trend (phenocrysts in lavas and cumulus phases in dunitic and wehrlitic nodules). In comparison, the 0.1 MPa experimental clinopyroxenes have higher Al_2O_3. Clinopyroxenes from VS96-54A charges (some olivine-added) are in the range typical of the most primitive natural diopsides (Mg# > 90, Al_2O_3 < 2 wt%).

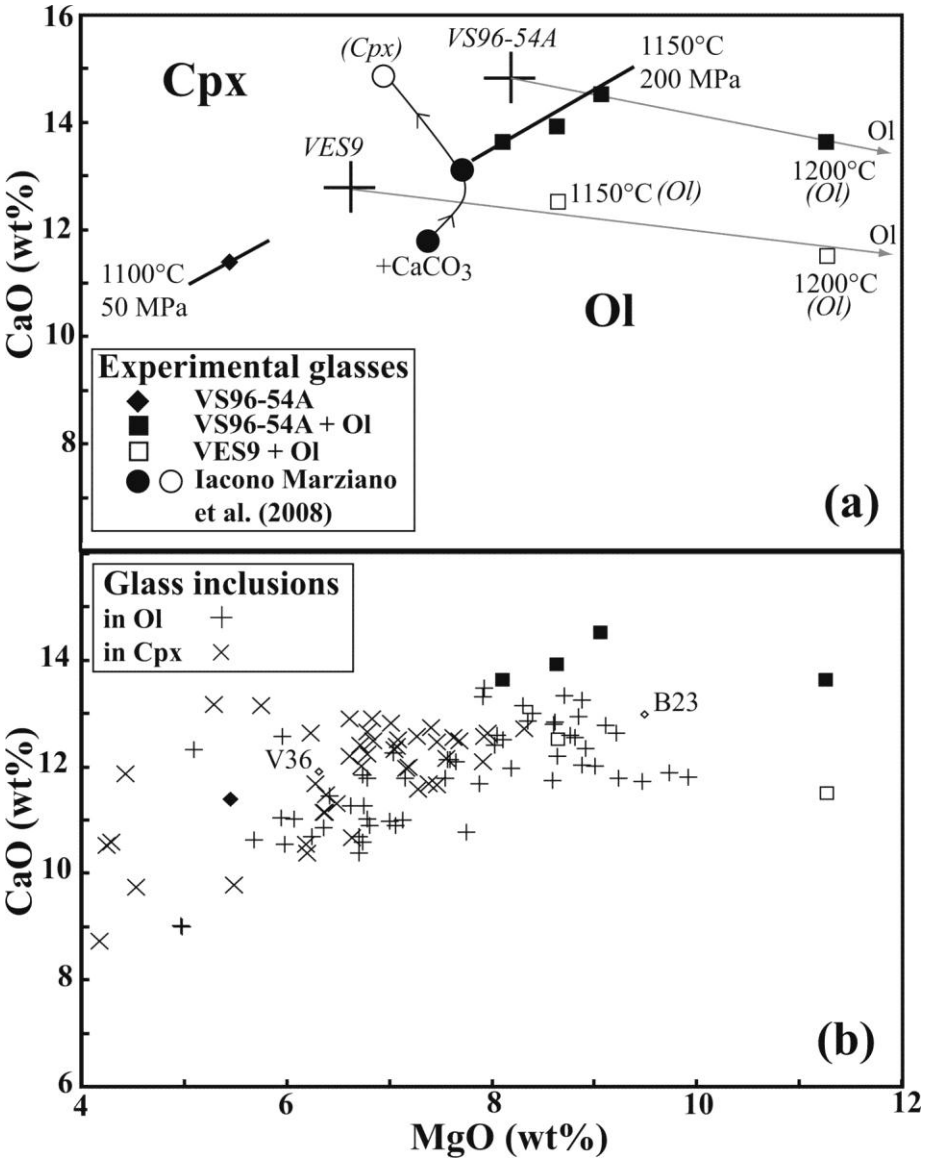

Fig. 9. CaO vs. MgO plot for (a) experimental glasses (Table 6) and (b) glass inclusions (recalculated compositions from Marianelli et al., 1995; 1999; 2005; Cioni, unpublished data, Cioni, 2000; Cioni et al., 1995; 1998; Fulignati et al., 2000; 2004b). The glass inclusion data are distinguished by type of host crystal (either Ol or Cpx). Experimental symbols indicate a cotectic phase assemblage (Ol+Cpx) when filled and single phase assemblages (either Ol or Cpx, phase assemblage specified next to the appropriate data points) when open. Experiments from this study are distinguished by starting material (either VS96-54A or VES9) and addition of olivine. See Tables 3-4 for more information about experimental conditions. The 1150°C, 200 MPa olivine + clinopyroxene cotectic is defined by the three VS96-54A olivine-added charges #5-1, #5-2, #5-3. One point of the 50 MPa, 1100°C cotectic is defined by the VS96-54A charge #7-1. The three olivine-bearing charges #5-4, #17-2, #18-1 are labelled with temperature (either 1150 or 1200°C). They plot on olivine control lines that extend from

the VS96-54A and VES9 starting glasses (Table 6) toward Fo-rich olivine (labelled Ol). Additional experimental glasses plotted are from three olivine- and $CaCO_3$-added charges ran at 1150°C, 200 MPa with a Stromboli basalt starting material (Iacono Marziano et al., 2008). The arrow indicates the direction of progressive addition of $CaCO_3$ (labelled + $CaCO_3$). Cpx and Ol (bold lettering) indicate the location of clinopyroxene and olivine primary phase fields. In (b), the composition of experimental glasses from this study, of tephrite V36 (Trigila & De Benedetti, 1993) and of Vulsini leucite basanite B23 (Conte et al., 2009; Table 7) are shown for comparison with the glass inclusions.

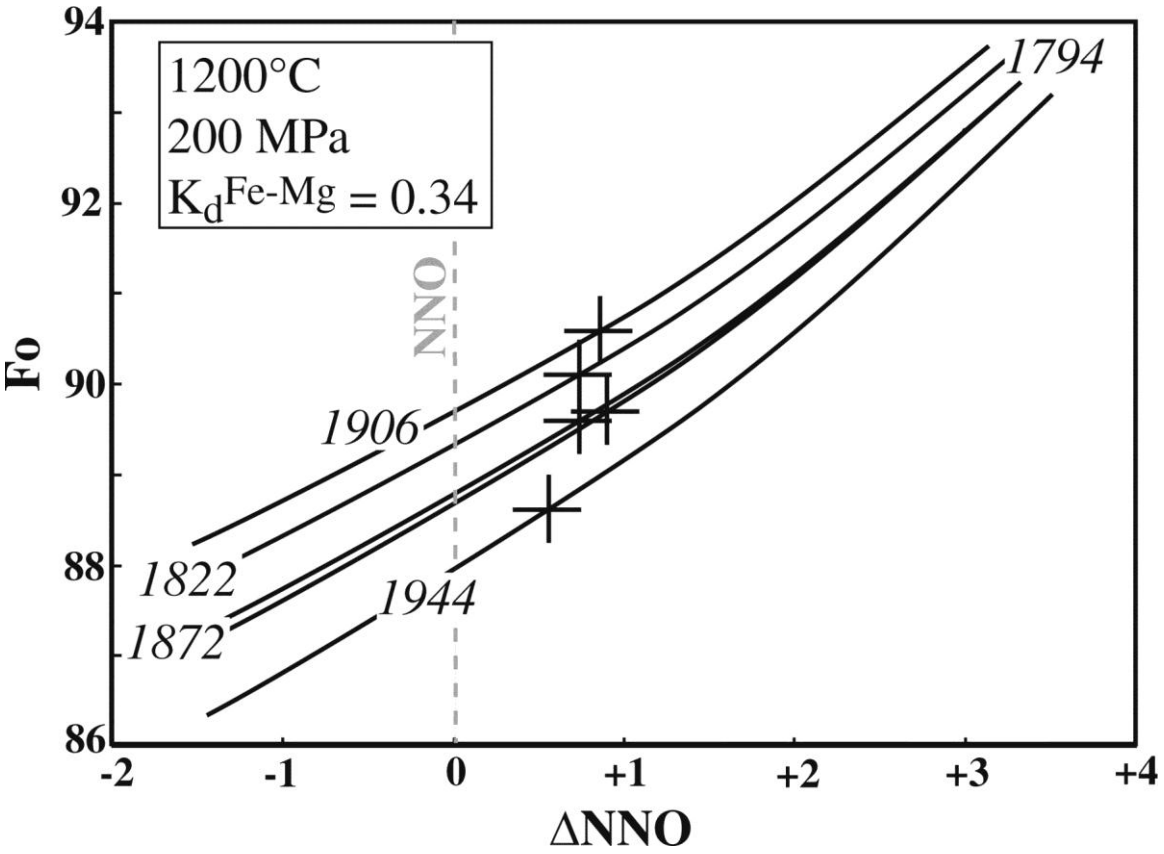

Fig. 10. Redox state of primitive Vesuvius liquids as constrained from olivine-liquid equilibrium. Each curve gives the Fo content of olivine at equilibrium with a given trachybasaltic liquid for different ΔNNO. Five trachybasaltic liquid compositions have been selected. They correspond to the most primitive glass inclusions from five different eruptions within the 1637-1944 period of activity of Vesuvius (recalculated compositions from Marianelli et al., 1995; 2005). The composition of their host olivine (Marianelli et al., 1995; 2005) is given by the five crosses. Chemical equilibrium is assumed between each trapped melt and its host olivine crystal, yielding a unique ΔNNO equilibrium value. Note the narrow range of ΔNNO (from +0.6 to +0.9) for the five glass inclusion-host olivine pairs selected. Despite significant differences in the composition of glass inclusions and olivines between

eruptions, all primitive magma batches appear to have equilibrated under similar redox conditions. All calculations are performed at 1200°C 200 MPa with an olivine-liquid K_d^{Fe-Mg} = 0.34 as determined in this study and for ΔNNO ranging from -1 to +3. ΔNNO (deviations from the NNO oxygen buffer) are calculated at 1200°C and 200 MPa (log fO_2 of the NNO buffer = -7.7, Pownceby & O'Neill, 1994). Liquid FeO contents are calculated from glass inclusion compositions using the model of Kress and Carmichael (1991).

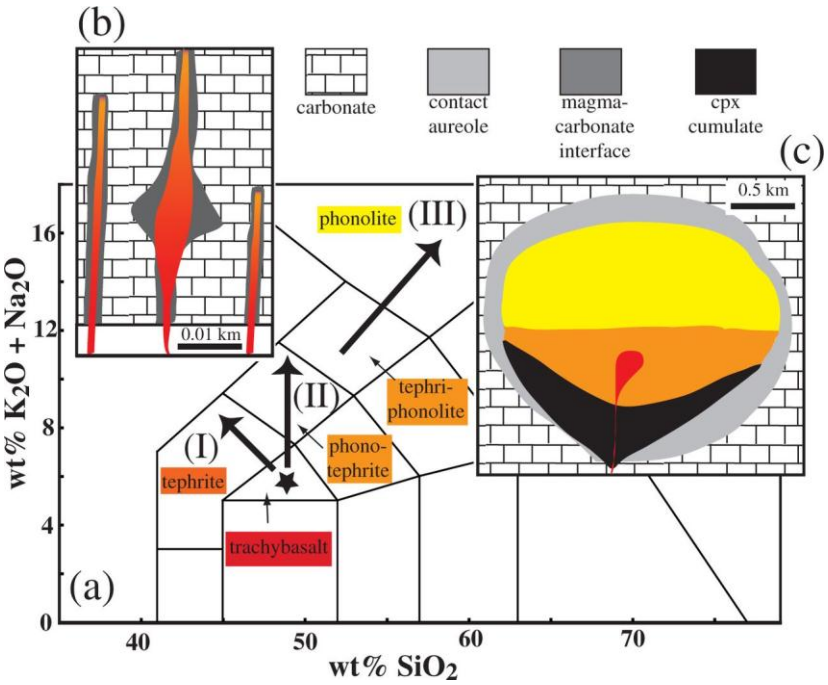

Fig. 11. (A) Total alkali – silica (TAS) plot showing the composition of parental magmas (black star) and the three main Vesuvius whole-rocks evolutionary trends. (I): carbonate assimilation; (II): complex open-system evolution; (III): closed-system crystal fractionation. (B) and (C): types of Vesuvius feeding systems (modified from Cioni et al., 1998). Type (B) describes the source of shallow reservoirs that feed open-conduit eruptions such as during 1637-1944 and in 1906 and 1944. Colour grading illustrates the progressive transition from trachybasalt to tephrite with carbonate assimilation. Products from those eruptions should be the most influenced by carbonate assimilation as shown by slightly negative to slightly positive whole-rock trends in the TAS diagram (Fig. 1b). Type (C) corresponds to large "mature" magma chambers tapped by Plinian eruptions such as Pompei and whose whole-rock evolutionary trends mainly reflect cpx fractionation, being on the whole little affected by carbonate assimilation. See text for more details.

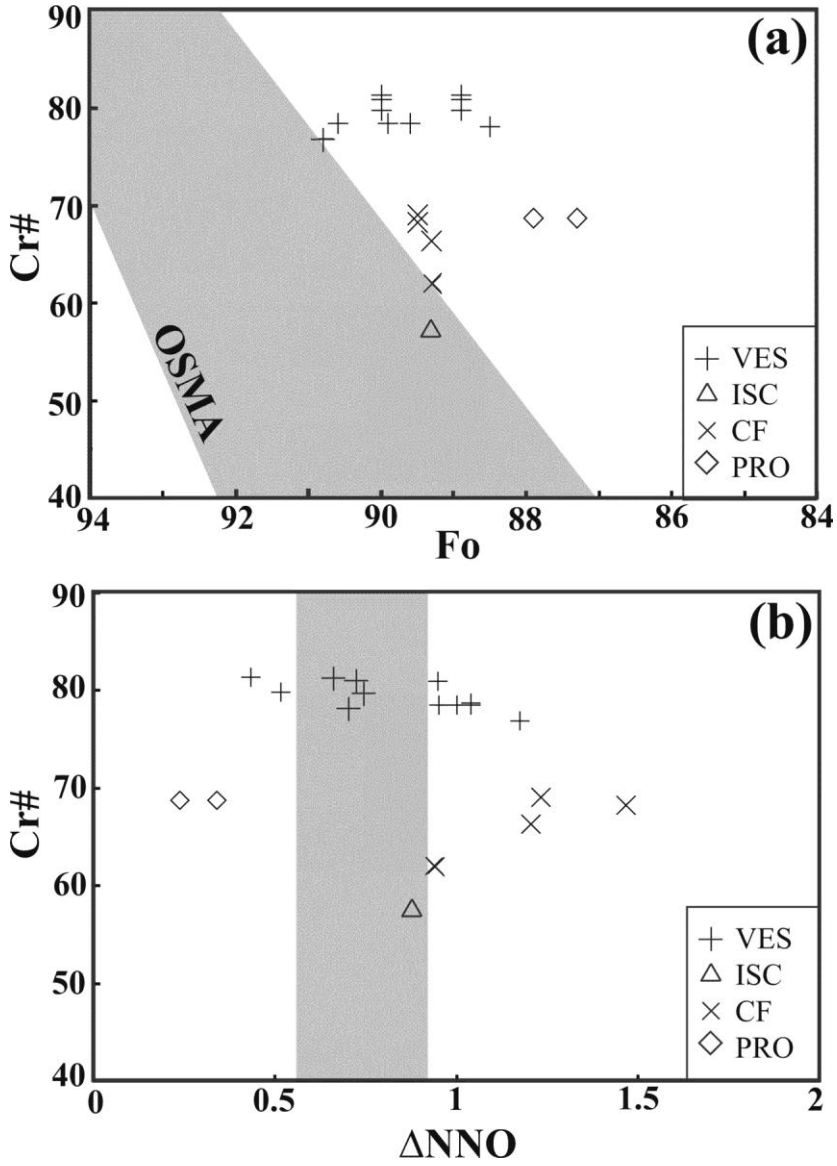

Fig. 12. Mineralogical characteristics (Cr# in spinel, Fo in olivine) and redox state (expressed as ΔNNO) of primitive Vesuvius magmas compared with other Campanian volcanoes. (a): Cr# in spinel vs. Fo in olivine; (b): Cr# in spinel vs. ΔNNO (calculated from the oxybarometer of Ballhaus et al., 1991). All calculations are carried out at 1200°C and 200 MPa (log fO_2 of the NNO buffer = -7.7, Pownceby & O'Neill, 1994). In (a), the grey field is the olivine-spinel mantle array (OSMA, Arai, 1994a; b). In (b), the grey field is the fO_2 range for Vesuvius determined from olivine-liquid (Fig. 10). Source of data: VES (Vesuvius, Marianelli et al., 1995; 2005; this study), ISC: Ischia (Vateliero eruption, D'Antonio et al., 2013), CF: Phlegrean Fields (Accademia Dome, Melluso et al., 2011), PRO: Procida (Solchiaro eruption, D'Antonio and Di Girolamo, 1994).